Chapter 4
Experimental Acoustic Modal Analysis of an Automotive Cabin

G. Accardo, M. El-kafafy, B. Peeters, F. Bianciardi, D. Brandolisio, K. Janssens, and M. Martarelli

Abstract In the automotive industry, one of the most important comfort requirements in designing a high quality vehicle is to avoid or minimize the noise in the passenger compartment. Therefore, an ever increasing interest exists to predict the interior acoustic behavior by means of accurate simulation models both to improve the vehicle NVH performance and to reduce the development cycle for new products. Nevertheless, nowadays the level of accuracy of such models is not sufficient to replace the design prototype phase with an all-digital phase, so experimental methods in which an acoustic characterization is performed based on measurements play an important role in understanding the modelling challenges, improving the overall modelling know-how and, more in general, in comprehension of the physical behaviour.

By means of a case study on a fully trimmed sedan car, this paper discusses the acoustic modal analysis equipment requirements and testing procedure. Due to specific acoustic modal analysis challenges, such as the high modal damping ratios and the need to use a large number of sound sources spread around the cabin to get a sufficient excitation of the modes, the modal parameter estimation is often a non-trivial task. Here the modal parameters (i.e. resonance frequency, damping ratio, mode shape, and modal participation factor) will be estimated by the new ML-MM method, a multiple-input multiple-output frequency-domain maximum likelihood estimator based on a modal model formulation. The performance of the ML-MM method will be compared to more classical modal parameter estimation methods.

Keywords Acoustic modal analysis • Interior car sound • Sound source • Fully trimmed sedan car • Vibro-acoustics effect

4.1 Introduction

In the past few decades, the reduction of interior noise levels in automotive cabins has become a very active research area, mainly encouraged by the need for weight reduction and the current trend towards environmentally compatible hybrid-electric power train concepts. Moreover the interior sound quality of a car is one of the most important decision factors for customers when purchasing a new car. Therefore, the interior sound quality has to be carefully considered and controlled in the design process. To improve the interior noise performance, CAE predictions have gained importance, especially in the early development stage when it is still possible to make changes without negatively affecting the vehicle development

G. Accardo (✉) • B. Peeters • F. Bianciardi • K. Janssens
Siemens Industry Software NV, Interleuvenlaan 68, B-3001, Leuven, Belgium
e-mail: giampiero.accardo@siemens.com; bart.peeters@siemens.com; fabio.bianciardi@siemens.com; karl.janssens@siemens.com

M. El-kafafy
Siemens Industry Software NV, Interleuvenlaan 68, B-3001, Leuven, Belgium

Acoustic and Vibration Research Group, Vrije Universiteit Brussel, Pleinlaan 2 B, B-1050, Brussels, Belgium

Faculty of Engineering – Mattaria, Helwan University, Helwan, Egypt
e-mail: melkafaf@vub.ac.be

D. Brandolisio
Siemens Industry Software NV, Interleuvenlaan 68, B-3001, Leuven, Belgium

Department of Mechanical Engineering, KU Leuven, Kasteelpark Arenberg 41-3001, Leuven, Belgium
e-mail: daniele.brandolisio@kuleuven.be

M. Martarelli
Faculty of Engineering, Università degli Studi eCampus, Novedrate, CO, Italy
e-mail: milena.martarelli@uniecampus.it

time. An acoustic finite element (FE) model of a vehicle cavity is an important component of a structural-acoustic numerical model for interior noise simulation. This model can be used to fine-tune the structural and acoustic design of the cavity to achieve specific NVH objectives. It can also be used as a diagnostic tool to identify the potential noise sources and also to evaluate the effectiveness of the proposed design modifications. It is obvious that the effectiveness of this approach greatly depends on the accuracy of the predictions made using such a model. Hence in order to understand the modelling challenges and improve the overall modelling know-how of which the car will benefit in the development phase, the experimental acoustic characterization of the cabin plays a crucial role. When performing an interior acoustic study, it is important to relate the acoustic responses to the intrinsic system behaviour of cabin cavity. This can be done by means of Acoustic Modal Analysis [1, 2], i.e. modal parameter estimation methods decompose the system behaviour into a set of individual resonance phenomena, each characterized by a resonance frequency, damping ratio, participation factor and mode shape. The experimental data set to derive this model from consists of a set of Frequency Response Functions (FRFs) between a set of reference (i.e. acoustic source input) degrees of freedom and all response (i.e. microphone output) degrees of freedom [3].

Specific acoustic modal analysis challenges are the high modal damping ratios resulting in highly overlapping modes with complex mode shapes and the use of a large number of references distributed around the cabin to get a sufficiently homogenous sound field.

Due to all these features, traditional modal parameter estimation methods may prove less suited for such data. Thus, a method overcoming the difficulties that the classical methods face when fitting an FRF matrix consisting of many (i.e. four or more) columns is needed. Recently, Yoshimura et al. published different studies on the experimental challenges related to the application of Acoustic Modal Analysis to an automotive cabin. They also proposed a non-linear least squares (NLS) method that is able to process FRF data with many references [4, 5].

This paper focuses on the experimental modal analysis of an automotive cabin. Here modal parameters will be firstly estimated by the well-known LMS Polymax method [6], and secondly by the ML-MM estimator, where the error between the modal model equation and the measured FRF data is minimized in a maximum likelihood sense [7, 8].

The paper is organized as follows. In Sect. 4.2 a brief overview about the theoretical background on Acoustic Modal Analysis is described. Using a discretized formulation, one can see that an analogy exists between acoustic and mechanical systems. Thanks to this equivalence, the classical approach can be used also in the acoustic modal analysis case, if one uses the correct variables. In Sect. 4.3 the case study on a fully trimmed car is introduced. Test preparation, set-up and measurements are described in detail. In order to have an idea on the expected acoustic modes, a numerical model was created and used for a preliminary analysis. This model was instrumental to study the proper distribution of sources and to prepare the geometry of the microphones capturing pressure response inside the cavity. Measurement points, sources and their respective location will be presented.

After the validation of the measurement chain, Sect. 4.4 discussed the modal parameter estimation. Two different methods are used for this purpose: firstly LMS Polymax and secondly ML-MM. Furthermore, a study on the influence of the number of references is carried out with Polymax and described in this section. The results previously obtained by the two methods are compared in terms of curve fitting, mean error, values of the modal parameters and mode shapes. Finally, in Sect. 4.5 some concluding remarks are given.

4.2 Theory of Acoustic Modal Analysis

In this section, only a brief theoretical overview is given. Many references can be consulted for further details about the model formulations describing the dynamic behaviour of (vibro-) acoustic systems, such as [9, 10].

Here boundaries of the enclosure will be modeled as rigid walls, so the dynamic behaviour of a pure acoustic system will be recalled.

By considering a three-dimensional closed acoustic system with rigid or finite impedance but non-vibrating boundaries, the governing equation of the system, excited by a point monopole of volume velocity at r_0 can be written in the form [9]:

$$\nabla^2 p\left(r, t\right) - \frac{1}{c^2} \ddot{p}\left(r, t\right) = -\rho \dot{q} \delta\left(r - r_0\right) \tag{4.1}$$

where p is the sound pressure, which is a function of space r and time t; c is the speed of sound; ρ is the density of the medium; and q is the volume velocity. The boundary condition over the rigid surface S is

$$\frac{\partial p}{\partial n} = 0 \text{ over } S \tag{4.2}$$

where n is the internal unit normal to S.

The discretization of the continuous acoustic wave equation is based on the finite element formulation. The acoustic domain of volume V is represented by an assemblage of acoustic finite elements. The pressure distribution within an element is interpolated in terms of the nodal pressures by using shape functions. Variational formulation based on the differential Eq. (4.1), boundary condition (4.2) and FE discretization gives the M^f, C^f and K^f matrices. To preserve the analogy with a structural finite element model, the matrix M^f is called the acoustic mass matrix, although it represents a compressibility matrix, relating the pressure to a displacement; the matrix C^f is the acoustic damping matrix, induced by the impedance boundary condition; the matrix K^f is called the acoustic stiffness matrix, although it represents an inverse mass or mobility matrix, relating the pressure to an acceleration. Assuming now that a number of point monopoles of known volume velocity are placed in the cavity and the sound pressure across the volume is sampled at an appropriate number of points, it can be shown that the continuous wave equation can then be substituted by its discrete equivalent:

$$M^f \ddot{p} + C^f \dot{p} + K^f p = -\rho \dot{q} \tag{4.3}$$

It is noted that in the present formulation, one-way coupling between the structure and the interior acoustic domain is assumed. This approximation is acceptable for the cases where the acoustic loading on the structures is negligible, like in automotive NVH applications, where air is the medium [11]. It can be seen that the discrete governing equation above is equivalent to the discrete mechanical equations of motions, with M^f, C^f, K^f in the role of mass, damping, and stiffness matrices; p in the role of displacement; and $\dot{q}$ in the role of force.

Taking the Laplace-transform and assuming zero initial conditions we get:

$$\left[s^2 M^f + s C^f + K^f \right] \cdot p(s) = -\rho s q(s) \tag{4.4}$$

As usual in structural dynamics, the inverse of the matrix term can be substituted by the frequency response function H(s):

$$p(s) = -\rho s H(s) \cdot q(s) \tag{4.5}$$

One can prove that the FRF-matrix can be expressed as a partial fraction expansion of modal parameters [12]:

$$H(s) = \sum_{r=1}^{N_m^f} \frac{Q_r \phi_r \phi_r^T}{s - \lambda_r} + \frac{Q_r^* \phi_r^* \phi_r^{*T}}{s - \lambda_r^*} \tag{4.6}$$

where N_m^f are the number of modes, ϕ_r the r-th modal vector, Q_r the modal scaling factor for the r-th mode, and λ_r the system pole for the r-th mode. Substituting now s by $j\omega$ and using Eq. (4.5) it is obvious that the modal parameters of the system can be gained from the FRF measurements where the sound pressures across the volume are referenced to the volume velocities of the sources. The expressions (4.4), (4.5), and (4.6) are in complete analogy with those being used in structural dynamics, therefore, it can be concluded that the classical modal parameter estimation approach can be followed also in the acoustic modal analysis case.

An interesting expansion towards coupled vibro-acoustic modal analysis is provided in [13].

4.3 Acoustic Modal Analysis Test Campaign

In this section, before describing the test campaign carried out to extract the acoustic modes of the cavity of a fully trimmed sedan car (Fig. 4.1) and extracting the modal parameters, a preliminary analysis with a Finite Element (FE) model is presented. Such a model will be used as a baseline to know the number and shapes of the acoustic modes of the system. The selected car for this case study is property of Siemens Industry Software and often used for NVH research purposes.

The description of the measurements will focus on the experimental set-up, its validation and the followed experimental procedure.

4.3.1 Preliminary Analysis

An acoustic FE model of the interior car cavity with rigid boundaries (Fig. 4.2) was created in LMS Virtual.Lab Acoustics, in order to know preliminarily the mode shapes and the number of acoustic modes expected in the frequency range of interest,

Fig. 4.1 Fully trimmed car used
in the case study

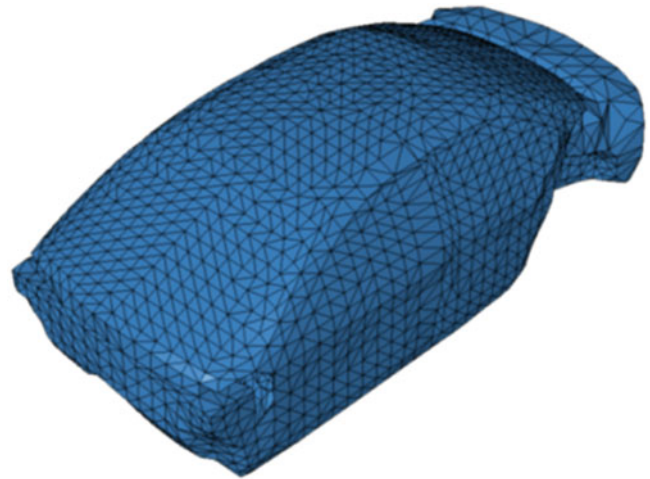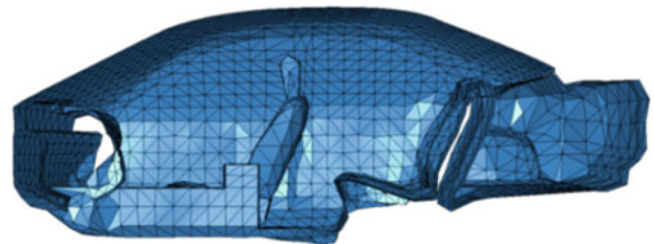Fig. 4.2 CAE cavity model

Fig. 4.3 Cavity cross-section

0–200 Hz. The internal cavity was modeled with more than 65,000 solid tetrahedral elements and more than 130,000 degrees of freedom. As visible in Figs. 4.2 and 4.3, the model includes also the geometry of the seats and the trunk compartment. Even though the rigid-walled assumption is not realistic due to the fact that the actual cabin consists of a number of flexible panels and surfaces with sound adsorbing material, the rigid-walled acoustic modes still provide a benchmarking for investigating the acoustic modal difference due to the structure-acoustic interaction [14]. Suitable physical characteristics of the air are defined for the fluid elements.

Hence under the assumption of rigid boundaries, the real eigensolution analysis shows that there are 10 uncoupled eigenmodes in the frequency range of interest (Table 4.1 and Fig. 4.4):

Let us highlight that the above model does not take into account any trim materials and any flexible boundary walls, so the eigenmodes from this rough model are not expected to be very close to the real ones. Nevertheless, at this first stage, this model is extremely useful to have an idea on the number of the modes and on their shape. Furthermore, information from the numerical model about the mode shapes are fundamental: (i) to know where to locate properly the sources in order to avoid nodal lines; (ii) to have a preliminary geometry of the measurement points; (iii) to select meaningful modes and address the dominant acoustic modes in such a coupled system where the FRFs are also influenced by the resonance of the structural system which has a rather higher modal density than the acoustic one [5, 15]. No FE model updating process will be performed on this model in the current paper, referring to possible future works for this purpose.

Table 4.1 CAE eigenfrequencies

#	Frequency [Hz]	Mode shape
1	≈0	Rigid body
2	44.53	I longitudinal
3	85.81	I longitudinal & rigid body trunk
4	112.42	I lateral
5	128.42	II longitudinal & rigid body trunk
6	141.06	I longitudinal & I lateral
7	150.20	I longitudinal & I lateral & I lateral trunk
8	155.57	I vertical
9	178.03	II longitudinal & I lateral & I lateral trunk
10	181.97	
11	201.20	I lateral & I vertical & I lateral trunk
12	205.98	III longitudinal

Fig. 4.4 CAE mode shapes – amplitude and phase
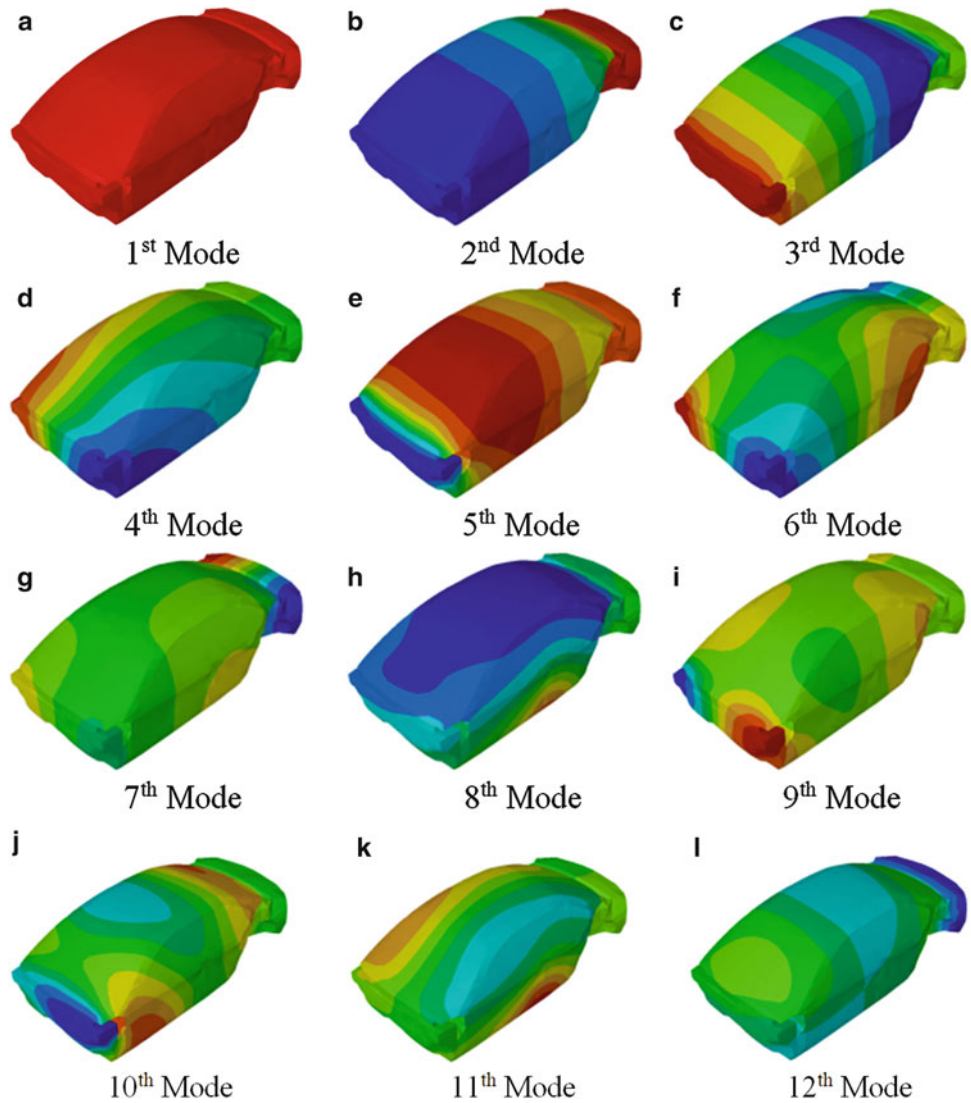
4.3.2   Experimental Set-Up

Multiple acoustic excitation tests were carried out inside the cavity of the sedan car already shown in Fig. 4.1. Thirty-four microphones located both on a roving array with spacing equal to around 20 cm and near to boundary surfaces captured the responses simultaneously. A total of 18 runs were performed to measure the pressure distribution over the entire cavity
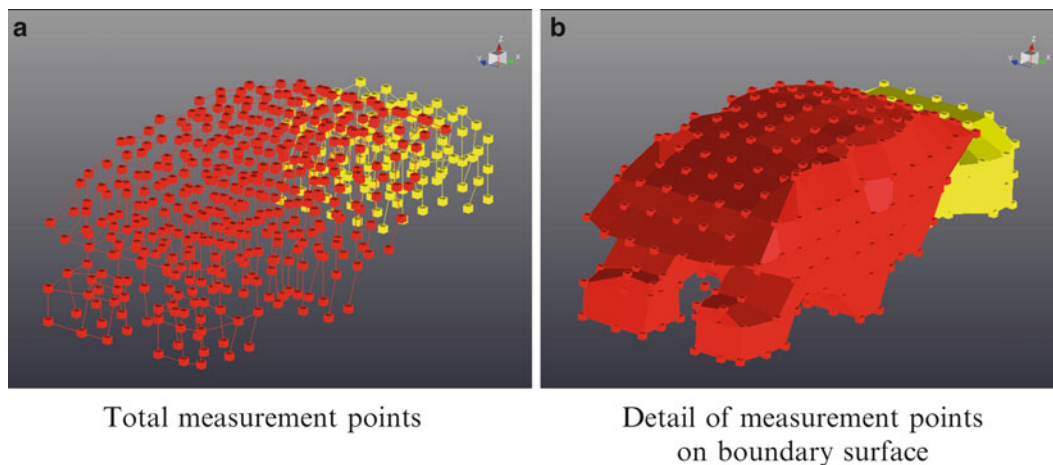
Fig. 4.5 Measurement points
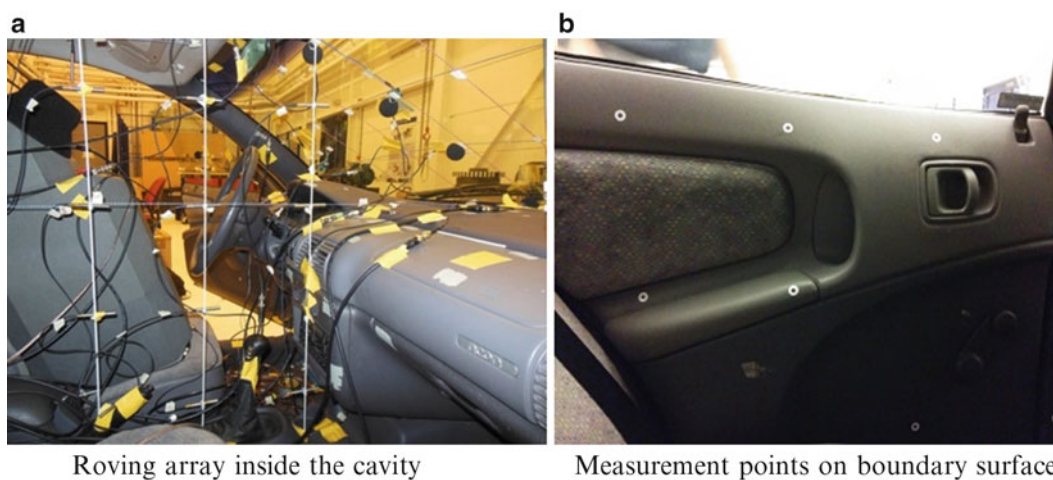
Fig. 4.6 Roving arrays

(both cabin and trunk). For each run, up to 12 loudspeakers switched on sequentially were used for acoustic excitation. A sequential excitation was preferred to a simultaneous excitation mainly to minimize the correlation between the inputs, and also the number of averages (hence time) to have good values of signal-to-noise-ratio [16].

In this section, a detailed description of the set-up used in the test campaign is given.

4.3.2.1　Measurement Points

The accurate description of the acoustic modes can be achieved by placing roving arrays of microphones at as different locations as possible in the vehicle, in order to increase the observability of the modes and to have more degrees of freedom to be used for the correlation and updating of the FE numerical model.[1] The pressure responses were measured both at the boundary surface and inside the cavity by positioning the microphones approximately every 20 cm (Figs. 4.5 and 4.6). The mesh of measurement points was preliminarily defined by means of the CAE model. Afterwards, the coordinates were updated to reflect the actual test scenario. Sensors were placed also in extreme positions, such as in foot regions, between the windshield and the dashboard, and in the hat shelf region, making a total of 526 measurement points. The same spacing and approach were followed for the trunk as well.

---

[1] A reasonable accuracy of the geometrical coordinates of the sensor locations is also need for the FE correlation and updating.

Fig. 4.7 Reference distribution

Side view

Front view

Back

Top view

Fig. 4.8 LMS Qsources

Miniature Volume Source (Q-IND)

Low Mid Frequency Source (Q-LMF)
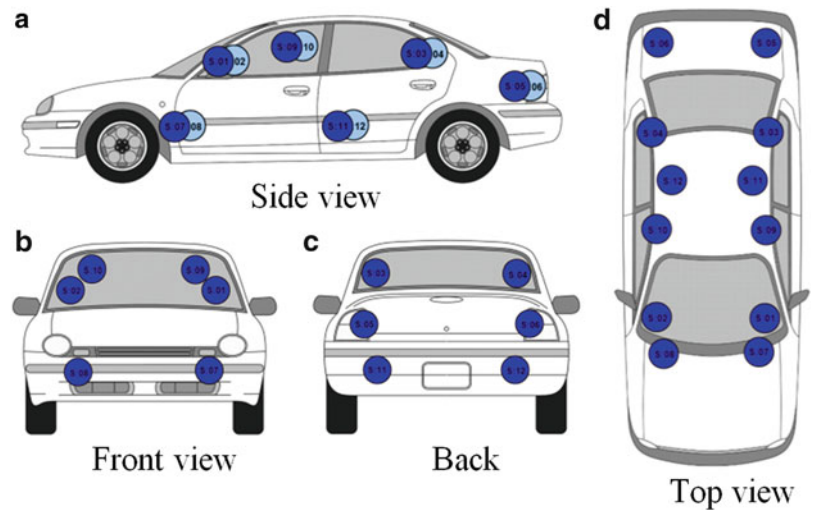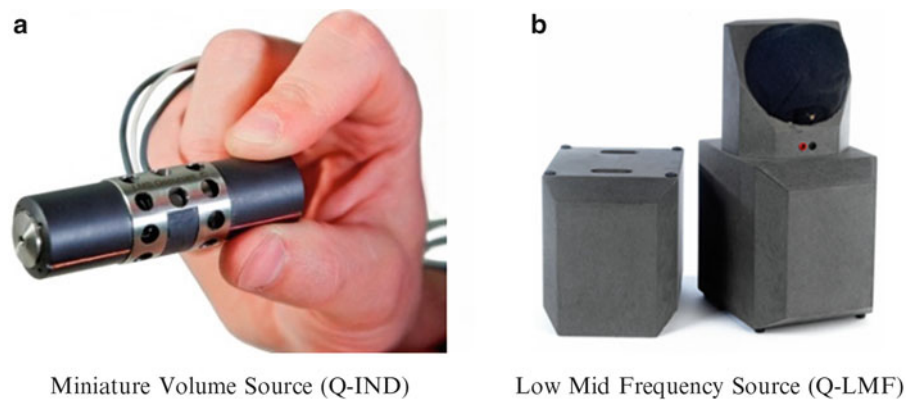
Twelve further microphones located 2 cm away from the acoustic sources were kept fixed to check the repeatability of the measurements. Additionally, four uni-axial accelerometers were placed on the structure at fixed locations again in order to check the repeatability and also to analyze vibro-acoustic coupling effects.

4.3.2.2 Sources

Calibrated volume acceleration sound sources are necessary to measure acoustic FRFs that are required in Acoustic Modal Analysis. Sound sources have to be omnidirectional and have a negligible size in order not to influence the field, above all in the higher frequency ranges [17]. As showed numerically in [3] and experimentally in [4, 5], an appropriate source distribution over the entire cavity is required to excite properly the acoustic modes. Indeed few sources do not allow the right identification of the mode shapes: distortions in the neighbourhood of the excitation point are strongly observed.

For this reason, a rather large amount of sources were used to excite as many modes as possible: up to 12 volume velocity sources were set in geometrically symmetric locations, close to the edges, corners and at the maximum amplitude locations to avoid nodal lines and excite close to pressure maxima on the boundaries. Locations of the mentioned excitation points are shown in Fig. 4.7.

Two different kinds of LMS Qsources (Fig. 4.8) were available: LMS Qsources Miniature Sources (Q-IND) and LMS Qsources Low-Mid Frequency Source (Q-LMF). The Q-LMF sources have the advantage to provide high noise levels of excitation (extremely high coherence) in low frequency range, but, on the other hand, they have the disadvantage to have a non-negligible size, as shown in Fig. 4.9. Nevertheless, the choice of using such sources was driven to the requirement of better exciting the lower frequency range. An analysis on the influence of these sources is reported below.

The **LMS Q-IND** sources have been developed to acquire acoustic and vibro-acoustic FRFs at low and mid frequencies in an accurate way without disturbing the acoustic behaviour of the passenger cavity. Due to its miniature size, such a source has no body diffraction and emits the noise as a monopole source in the frequency range between 50 and 5,000 Hz. As shown
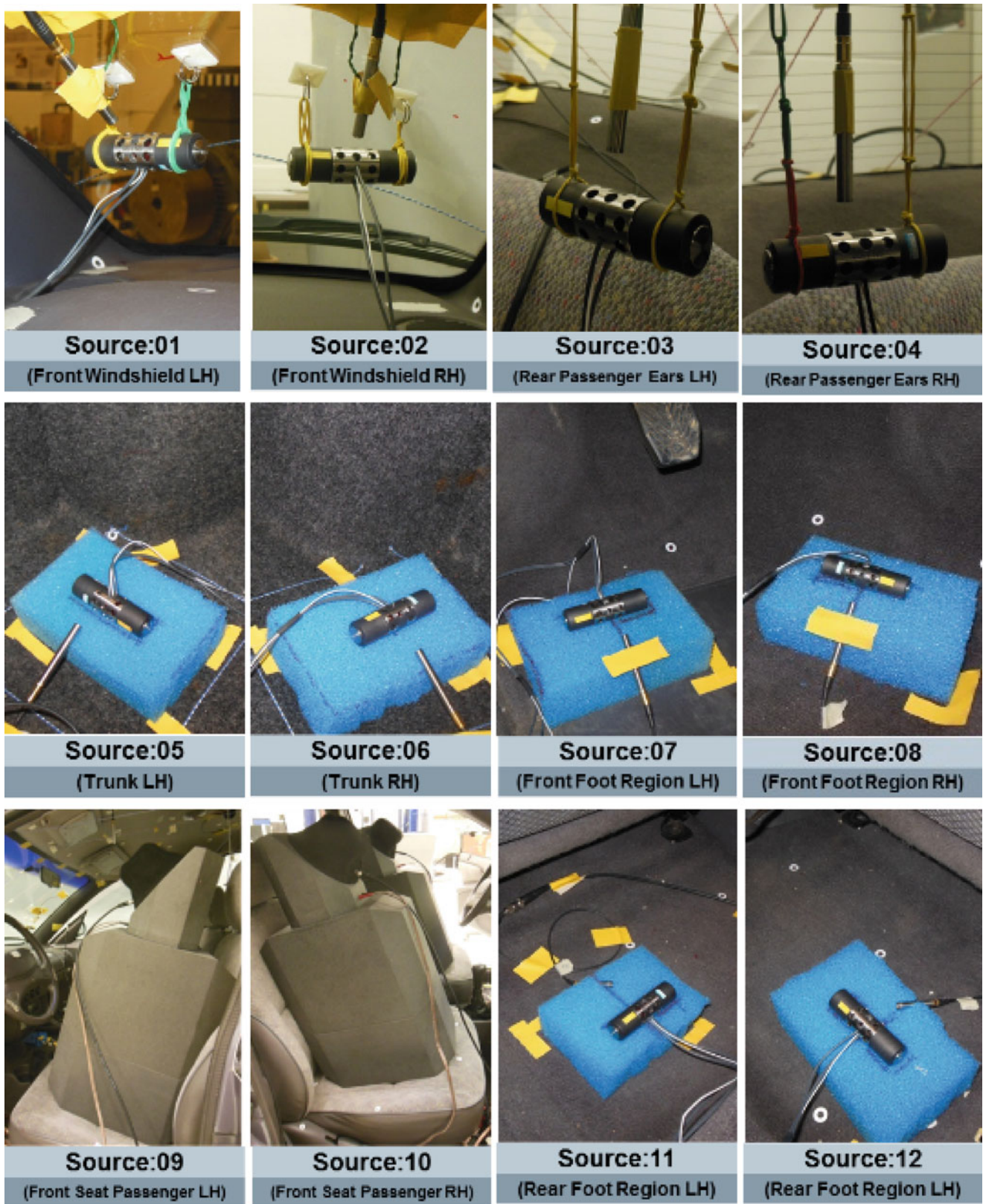
Fig. 4.9 Source locations

Fig. 4.10 Q-IND: directivity of the sound source
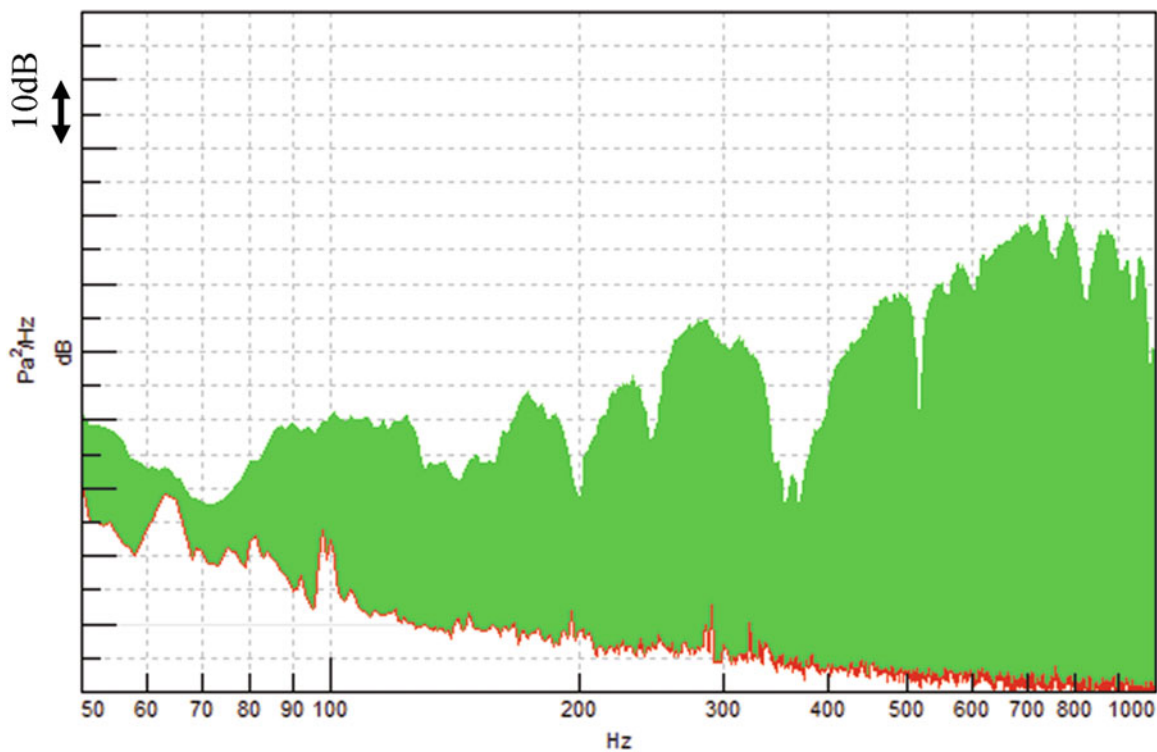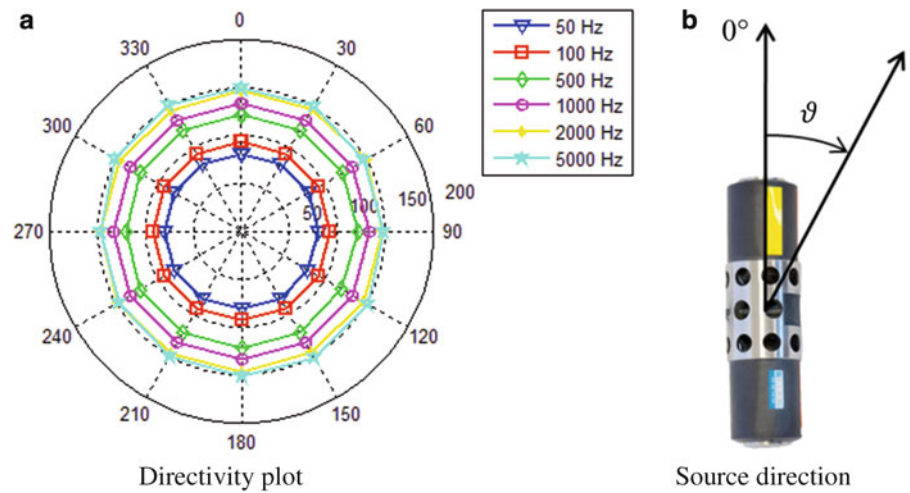

Directivity plot   Source direction

Fig. 4.11 Q-IND: noise level versus background noise

in the directivity plot[2] in Fig. 4.10, the emitted sound does not attenuate along different directions up to several kHz; hence the source can be properly used as a monopole. The source incorporates electro-dynamic actuators and an internal sound source strength sensor. It outputs a volume displacement signal.

Figure 4.11 shows a comparison between a microphone response in the trunk when the source is active and when the source is switched off. Above 50 Hz, the artificial noise generation results in a response that is up to 50 dB higher, at certain frequency lines, guaranteeing a sufficient signal to noise ratio necessary for an accurate FRF measurement.

---

[2]The directivity plot is based on FRF in 1/3 octaves by using white noise as excitation signal. The distance from the sound-source to the recording microphone was 50 cm in semi free-field condition. The measurements have been carried out in semi-anechoic test laboratories at the LMS Engineering Services facilities in Belgium.
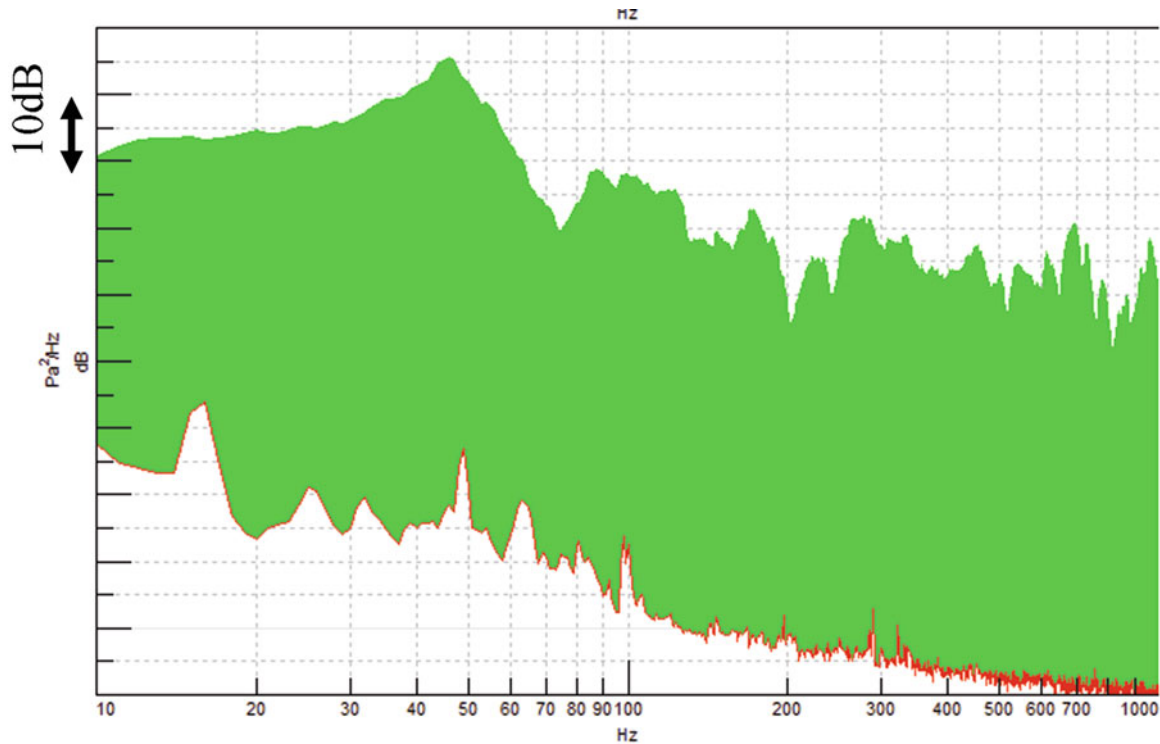
Fig. 4.12 Q-LMF: noise level versus background noise

The **LMS Q-LMF** sources are designed to be used in the frequency range between 10 and 1,000 Hz covering an important frequency band in vehicle development. Because most applications are for seat positions, these devices are optimized for quick positioning on a seat with the acoustic center at ear location (compliant with ISO5128). The unique properties of this low/mid-frequency source include compact, human body diffraction simulation, omnidirectional, time-stable sensitivity and high noise levels compared to measured background noise, as visible in Fig. 4.12.

Coster et al., in [18], reported that the effect of the source body diffractions and source directivity are negligible up to 100 Hz in free-field condition. As visible in Fig. 4.13, the presence of these sources inside the cavity influences the acoustic field from 80 Hz onwards.

So it's worth to underline that the FRFs will be partially affected by the presence of the Q-LMF sources. For this reason, Q-LMF have been kept fixed on the front seats during the whole test campaign in order not to introduce measurement data inconsistencies by varying volume distortions. However, a numerical simulation taking into account the sources located as in the real scenario (Figs. 4.14 and 4.15), has shown that the eigenfrequencies are only slightly shifted in the frequency range of interest. Comparing the eigenfrequencies in Table 4.2, one can observe that the maximum relative error between the values of the two models is always less than 3 % for the first eight modes. Furthermore, the MAC values in Fig. 4.16 are really near to 1, hence the mode shape distortion is still reasonable, for the first eight modes. Let's note, from Table 4.2 and Fig. 4.16, that only the 9th and 10th modes are mainly influenced by the presence of the Q-LMF sources: their order seems to be switched.

Hence error on the measurements due to the presence of such bigger sources can be considered rather limited.

Further details about source performances will be shown in the next section.

4.3.3 Set-Up Validation

4.3.3.1 Excitation Signal Level

The quality of modal analysis relies critically on the quality of the measured FRFs. So assessment on the quality of experimental data becomes essential. Hence, before starting the actual testing, a first set of measurements was performed to validate requirements such as efficiency of the inputs, reciprocity, repeatability and linearity.
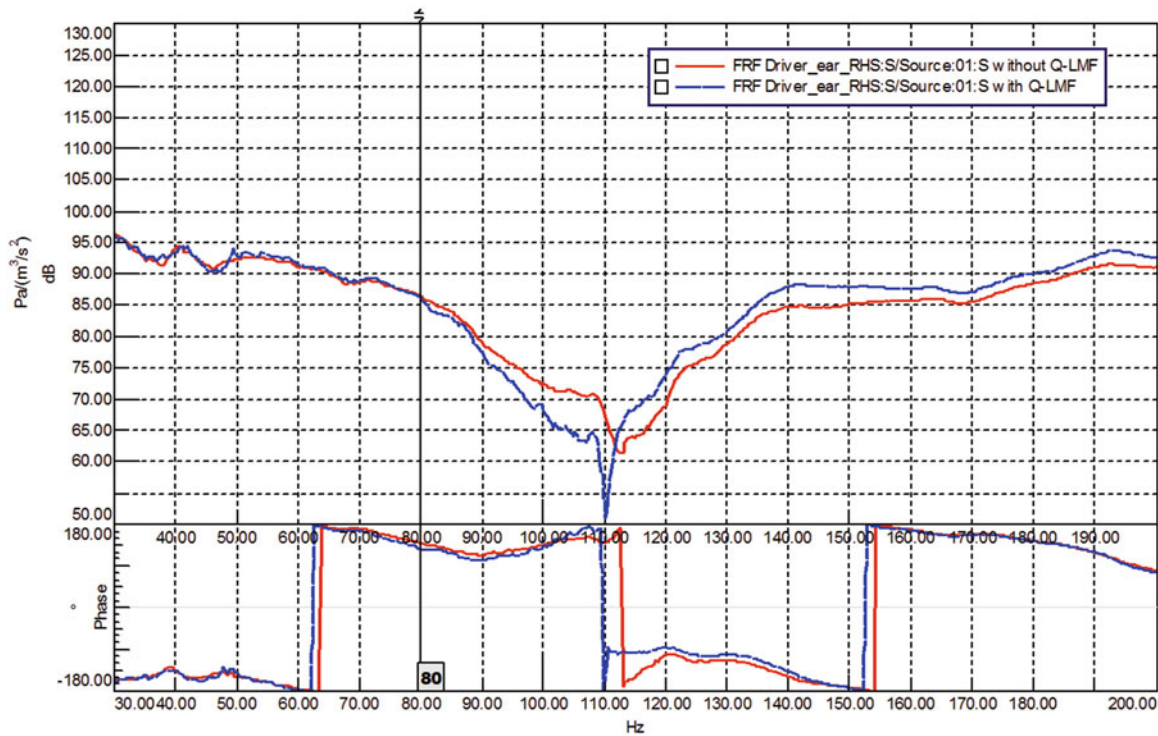
Fig. 4.13 Volume distortion due to the presence of Q-LMF sources

Continuous random white noise was chosen as excitation signal. The H1 estimator was used to compute the FRFs based on 150 averages.

Typical input autopower spectra expressed in volume acceleration are shown in Fig. 4.17. One can observe that an acceptable level of energy goes into the system over the frequency band of interest.

4.3.3.2 FRFs Reciprocity

Because of the symmetry, the FRF matrix, which is mathematically the inverse of the dynamic stiffness matrix, will also be symmetric. Hence FRF data from a measurement should be identical if we exchange the locations of input and output. Theoretically, this property can be traced back to the symmetry of mass, stiffness and damping. Reciprocity was checked in order to assess the reliability and accuracy of the measured FRFs. Figure 4.18 shows an example of reciprocity check: one can see that the amplitude and phase are nearly the same for both cross frequency response functions over the whole frequency range of interest.

4.3.3.3 Repeatability

Since during the test procedure doors and trunk were opened several times, the repeatability of the measurements was constantly monitored throughout the entire test campaign. This was mainly to ensure that the dynamic behaviour of the system and the whole measurement set-up system were time-invariant [19, 20]: certain FRFs were measured for each run, just to check the that neither the system nor the test set-up have experienced any significant changes. Figure 4.19 shows that the dynamic behaviour of the system was constant and that the testing conditions were kept unaltered throughout the measurement.

Fig. 4.14 Model with Q-LMF sources – CAE mode shapes (amplitude and phase)

a 1st Mode

b 2nd Mode

c 3rd Mode

d 4th Mode

e 5th Mode

f 6th Mode

g 7th Mode

h 8th Mode

i 9th Mode

j 10th Mode

k 11th Mode

l 12th Mode
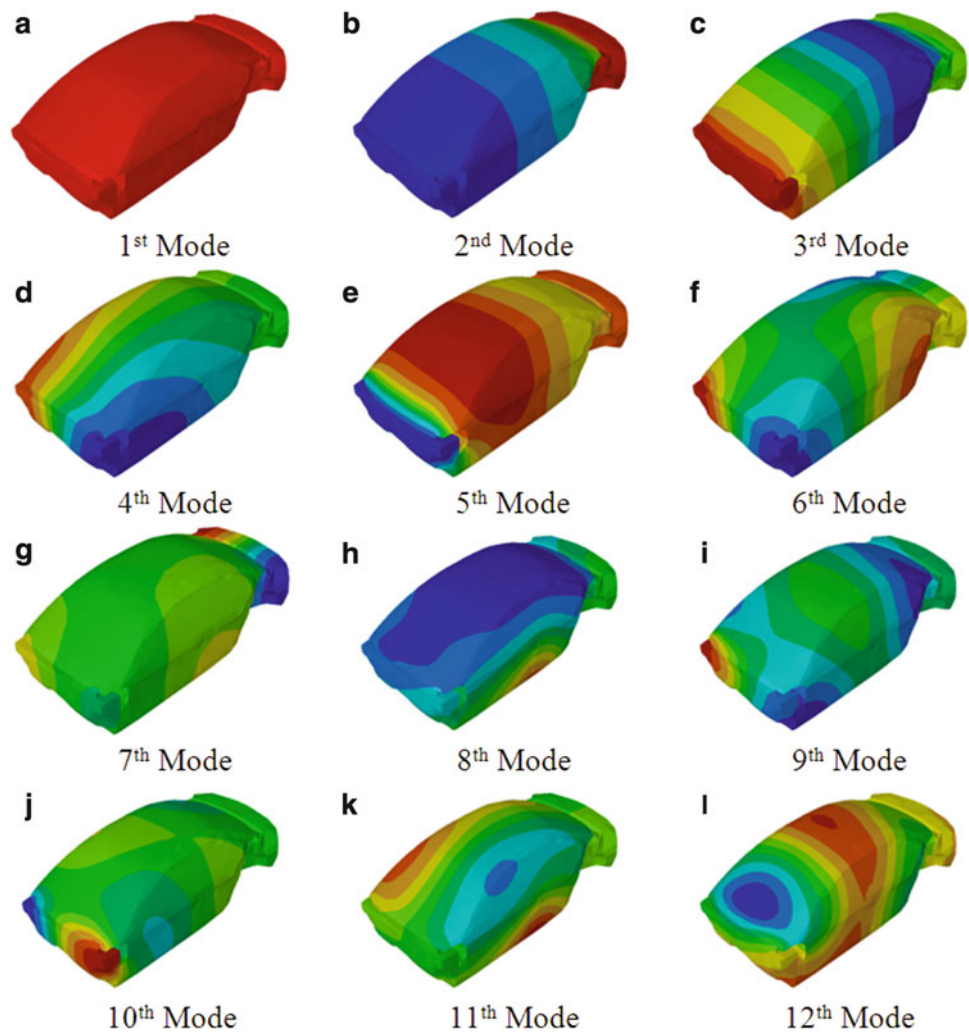
Fig. 4.15 Cavity cross-section and Q-LMF location
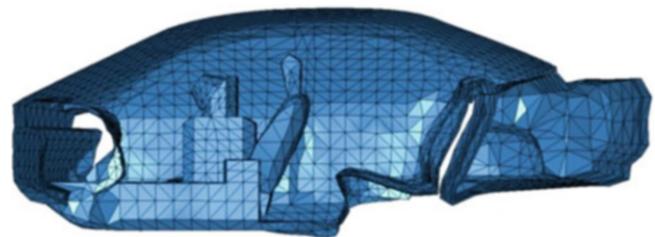
4.3.3.4 Linearity

As a last check, the linearity of the system was tested: measuring the FRFs at difference force levels can partly check non-linearity. Indeed if the system is linear, FRFs are independent of excitation amplitudes. As visible in Fig. 4.20, the FRFs from the same location measured with different excitation levels show the uniformity of the curve and the linear behaviour of the system.

The validation of the entire measurement chain has proven the good quality of the measurement method being used. By checking the auto-powers of the inputs, the cross frequency responses (reciprocity), the consistencies of the data throughout the measurements (repeatability) and the system responses for different input levels (linearity), the proper excitation of the system, the reliability of the inputs, and the assumption of time-invariant linear system are guaranteed.

Table 4.2 CAE model without Q-LMF vs. CAE model with Q-LMF

#	CAE model without Q-LMFs		CAE model with Q-LMFs	
	Frequency [Hz]	Mode shape	Frequency [Hz]	Mode shape
1	≈ 0	Rigid body	≈ 0	Rigid body
2	44.53	I longitudinal	44.72	I longitudinal
3	85.81	I longitudinal & rigid body trunk	84.19	I longitudinal & rigid body trunk
4	112.42	I lateral	109.42	I lateral
5	128.42	II longitudinal & rigid body trunk	130.10	II longitudinal & rigid body trunk
6	141.06	I longitudinal & I lateral	140.07	I longitudinal & I lateral
7	150.20	I longitudinal & I lateral & I lateral trunk	149.98	I longitudinal & I lateral & I lateral trunk
8	155.57	I vertical	153.53	I vertical
9	178.03	II longitudinal & I lateral & I lateral trunk	177.37	
10	181.97		178.80	II longitudinal & I lateral & I lateral trunk
11	201.20	I lateral & I vertical & I lateral trunk	199.71	I lateral & I vertical & I lateral trunk
12	205.98	III longitudinal	204.00	III longitudinal

Fig. 4.16 CAE model without
Q-LMF vs. CAE model with
Q-LMF – MAC matrix
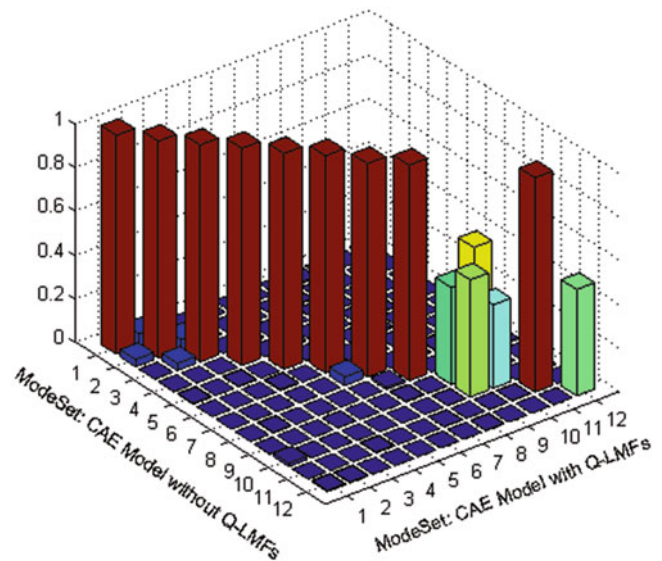
4.4   Experimental Modal Analysis

In this section the modal parameters of the cavity are firstly estimated by LMS Polymax. A study on the influence of the number of references is performed and the main challenges of analyzing acoustic modal analysis measurement data are presented.

Secondly the new frequency-domain maximum likelihood estimator based on a modal model formulation (ML-MM) is applied to the case with 12 references and the modal parameters are compared with those estimated by the previous method.

4.4.1   Results with Polymax and Influence of Number of References

An important issue to be addressed when processing acoustic modal analysis data is the identification of pre-dominantly acoustic modes in FRFs with a rather high modal density. Even if purely acoustic FRFs have been measured, the modal density is high since the acoustic cavity is coupled to a flexible body and also the resonances of the structural system (mainly panel vibrations from the windshield, the roof, . . .) show up in the microphone measurements. So, as already observed in [4], among the several coupled natural frequencies, the number of effective acoustic eigenvalues must be narrowed down to a level that is around the number of uncoupled acoustic eigenvalues computed analytically or numerically. For this purpose the data acquired by accelerometers placed on strategic positions (windshield, roof, trunk, side windows, . . .) can help to
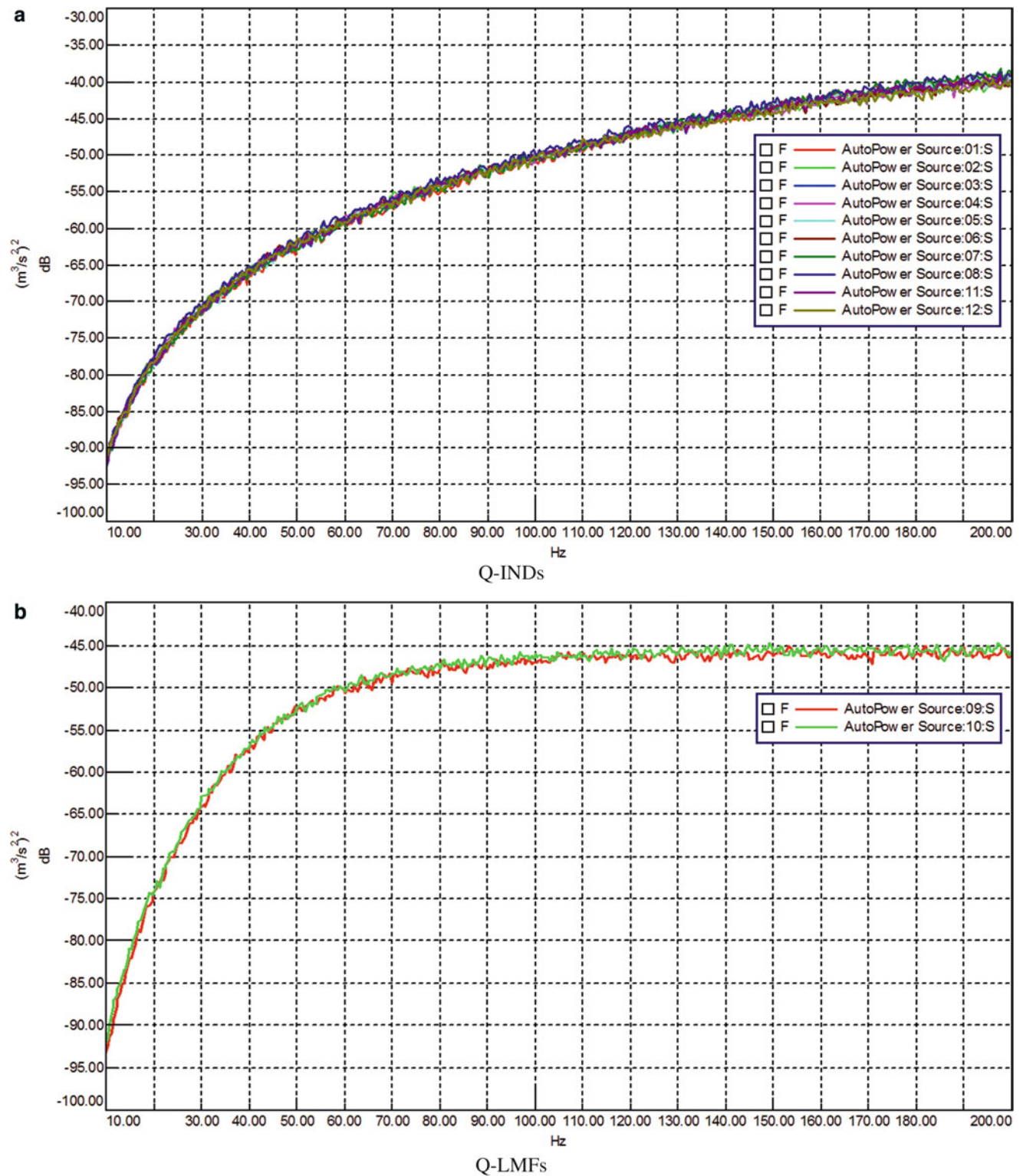
Fig. 4.17 Autopower spectra with continuous random white noise excitation

distinguish the dominant acoustic modes: analyzing the structural driving points FRFs, the main peaks in these FRFs can be considered to be structural modes. If these frequencies are also revealed in the acoustic FRFs, then they can be assumed as not purely acoustic. Moreover, the high damping of the cavity involves lower and wider peaks in FRFs resulting in highly overlapping modes. Finally, possible data inconsistencies, due to the fact that the different runs were performed in different
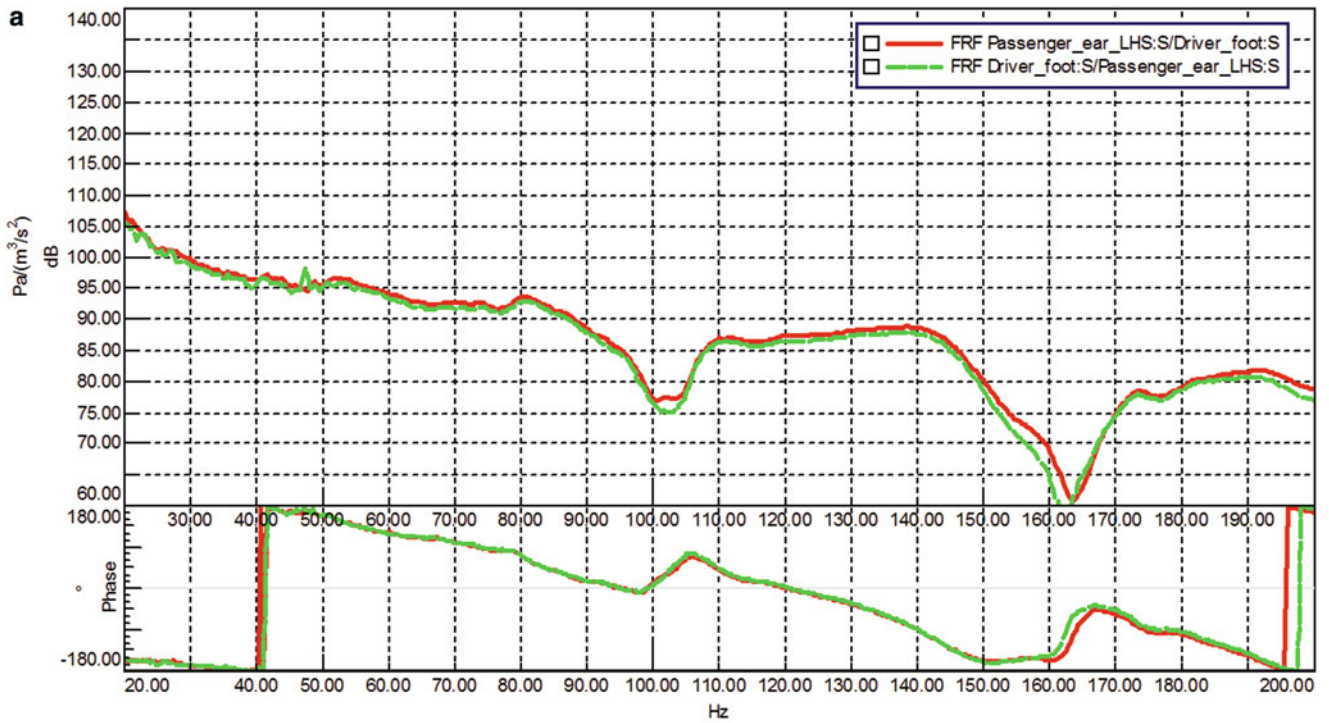
Passenger_ear_LHS – Driver_foot reciprocity
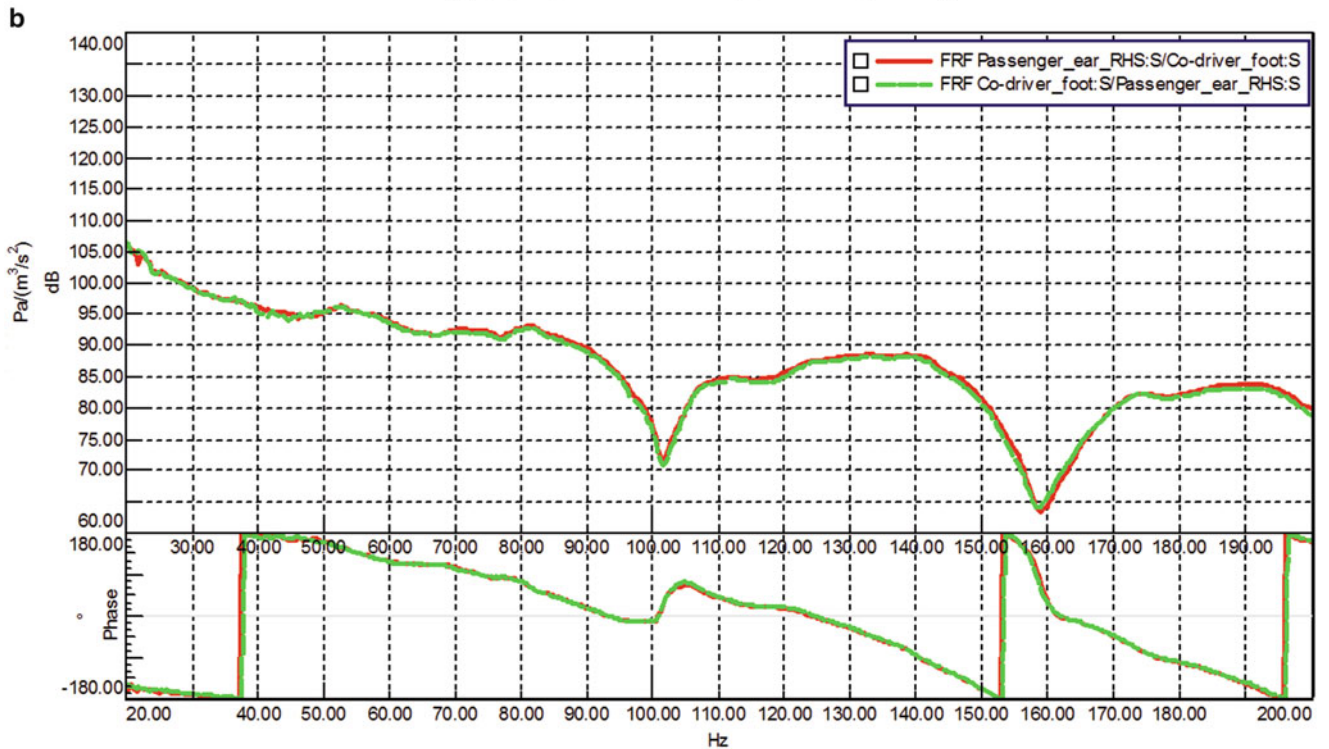
Passenger_ear_RHS – Co-driver_foot reciprocity

Fig. 4.18 Reciprocity check
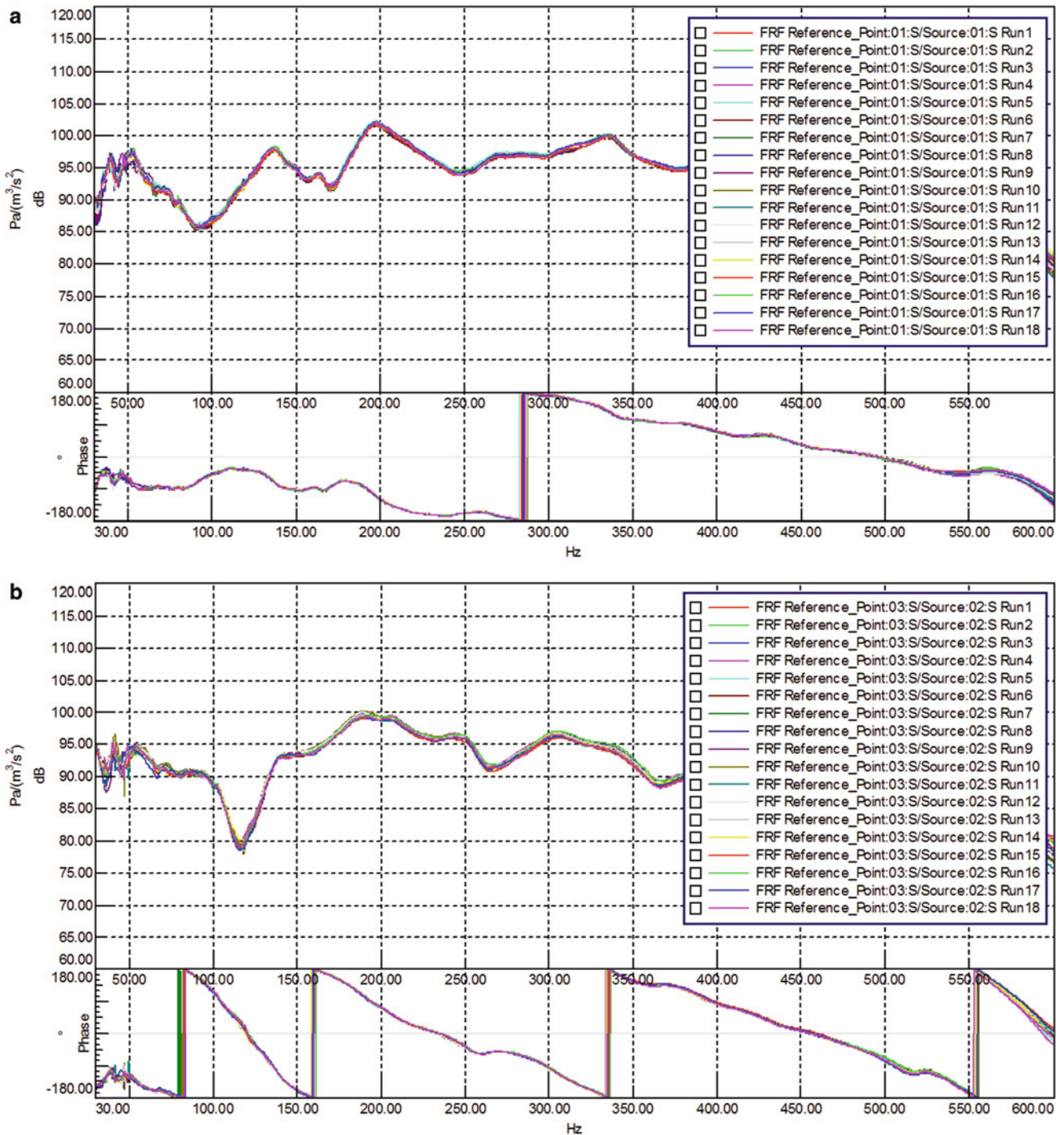
Fig. 4.19 Examples of repeatability check

days, can cause resonance frequencies to vary within the test database and when analyzed altogether, can cause a rather unclear stabilization chart, and hence a non-trivial selection of the right stable pole – or more precise, the right stable pole does not exist as such, there are multiple stable poles identifying the same mode.

As already said, a further difficulty to identify acoustic mode shapes is also due to the shortage of speakers to excite all the dominant modes [5]. Hence different cases, with 6, 10 and 12 references (Fig. 4.21), are analyzed in order to study the influence of number of references on the proper excitation of the acoustic modes.
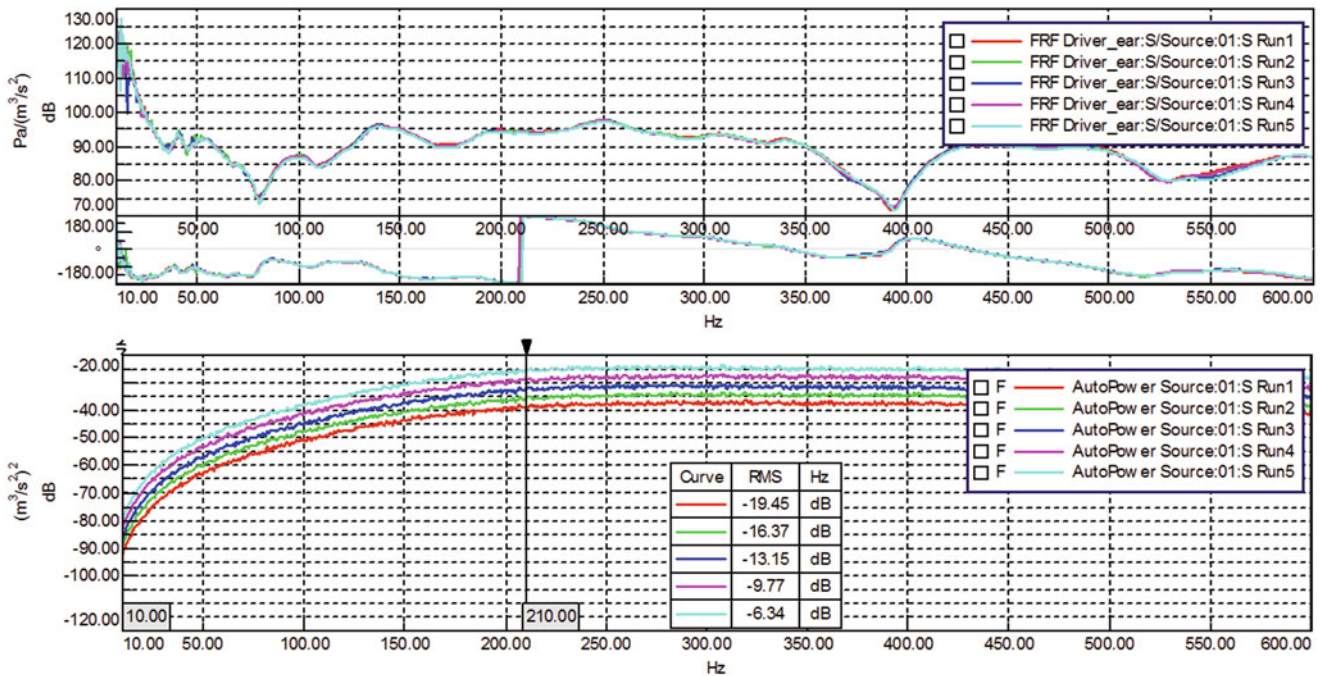
Fig. 4.20 Linearity check
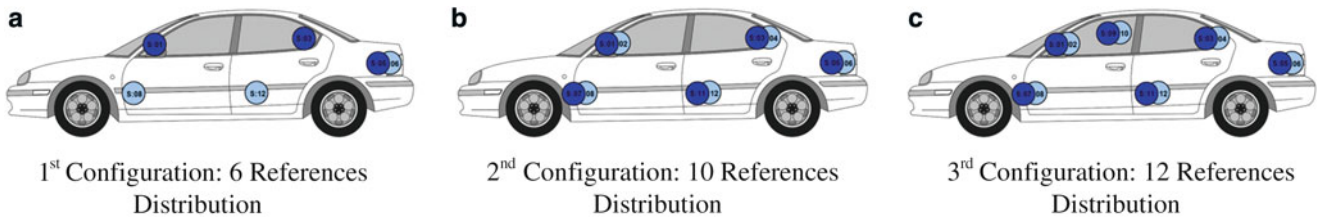
Fig. 4.21 References layouts

Whereas the Q-LMF sources are able to excite well the low frequency range, resulting in a really high coherence from 15 Hz onwards (Fig. 4.22b), the Q-IND sources can emit a strong signal only from 50 Hz onwards. The coherence is indeed rather low up to 30 Hz (Fig. 4.22a). Hence modal parameters are extracted in the frequency range from 40 to 200 Hz, excluding the acoustic rigid body mode (1st Mode) around 12 Hz.

Modal parameters are extracted using a total of $526 \times N_i$ (with N_i the number of references in each configuration) FRFs simultaneously. Nine pure acoustic modes are well identified in this frequency range with 12 references (Fig. 4.23). Most of the expected modes are extracted in the 3rd configuration, whereas 1 mode is not extracted in the 1st configuration. A global improvement of the mode shapes is observed when increasing the number of references: the nodal lines become clearer and mode shapes gain more symmetry. On average, one can see that out of diagonal elements of AutoMAC matrix get lower when increasing the amount of references, as a result of a less correlation with themselves. Figures 4.24 and 4.25 show an example of this general trend. In Table 4.3, the results obtained for each configuration are summarized. Let's observe that all the modes below 140 Hz are always successfully identified, whereas an increasing number of references is needed to better extract the pure acoustic modes in higher frequencies. Finally, one can observe that three adjacent modes around 150 Hz are well extracted in the last two configurations. Nevertheless, their order is a bit different in the two cases (Fig. 4.26).

As experienced before, it was quite challenging for classical modal parameter estimation methods to curve-fit an FRF matrix with so many columns (12 references) (Fig. 4.27). The mean fitting error was around 9 % for the 3rd configuration, so modal data could be affected by a non-negligible error. Therefore, a new iterative frequency-domain solver that has the potential to overcome the difficulties with many references was also used and briefly illustrated in the next section.

Q-IND (Source:01)

Q-LMF (Source:09)
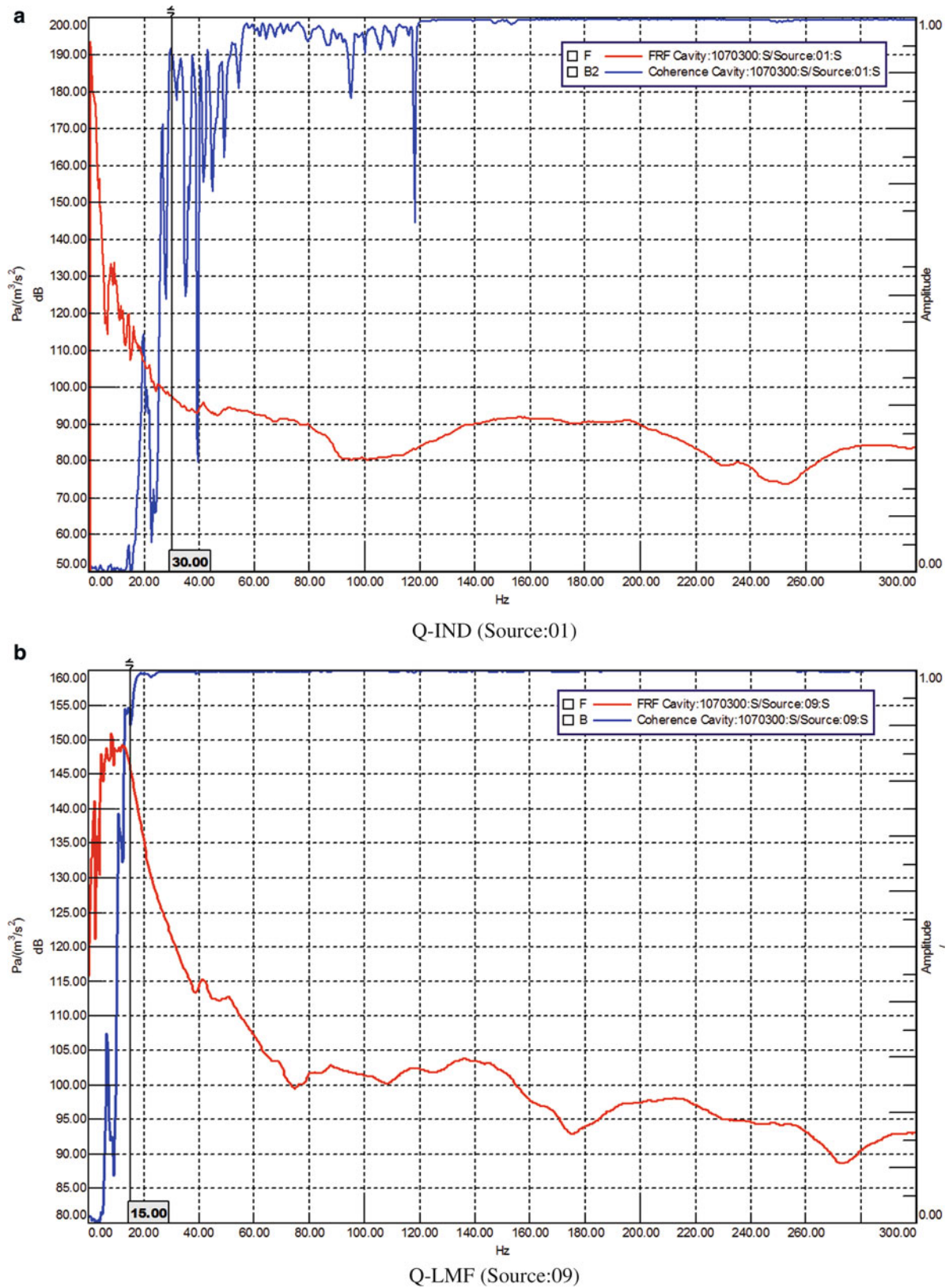
Fig. 4.22 Some coherence examples
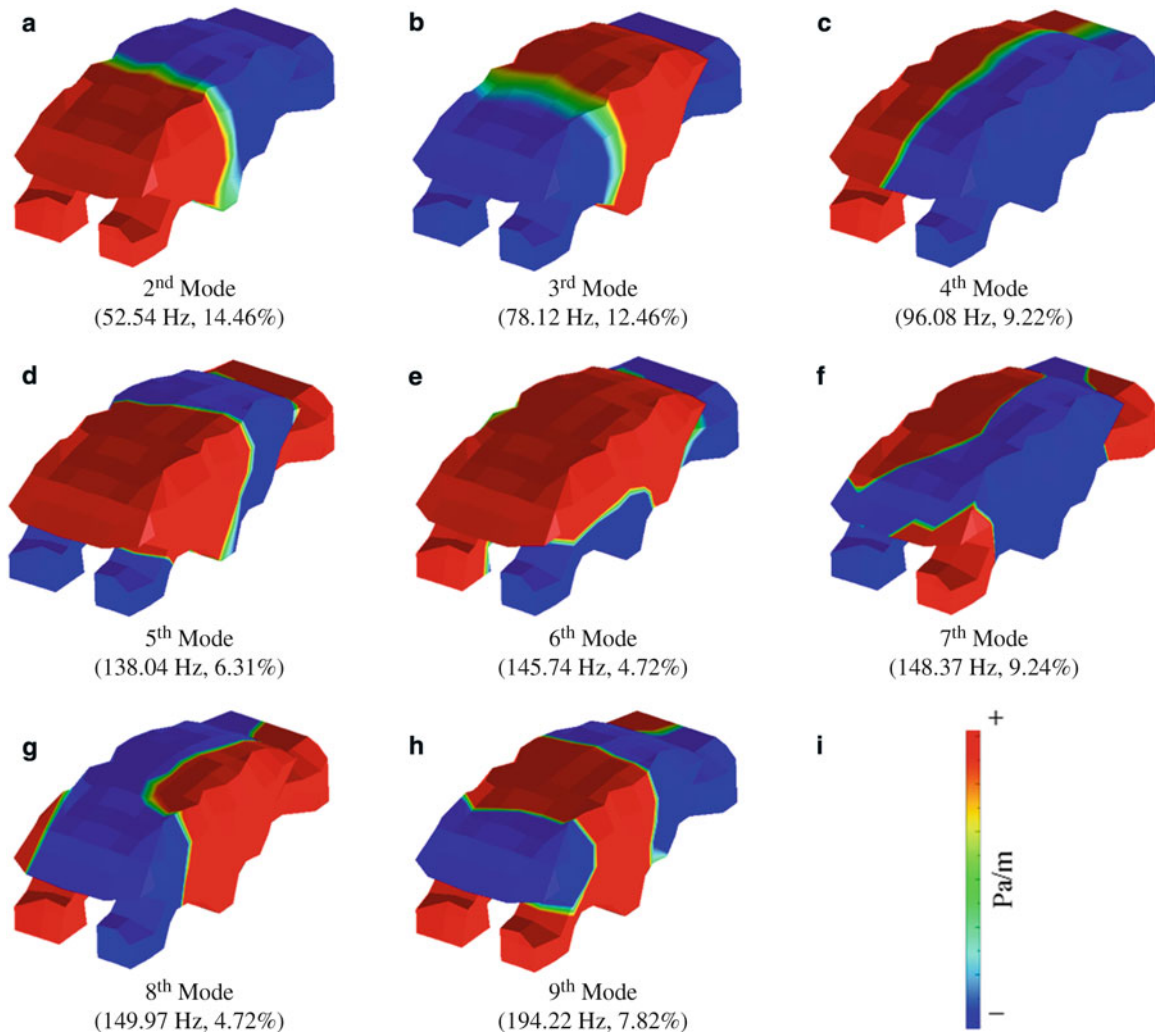
Fig. 4.23 Mode shapes – amplitude and phase (12 references)

Fig. 4.24 II longitudinal mode
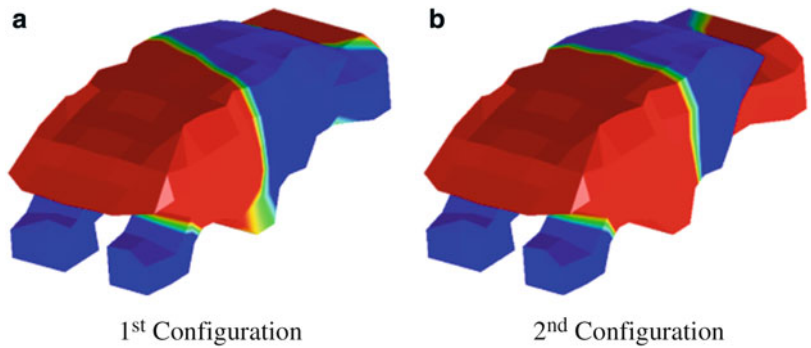
4.4.2 Maximum Likelihood Estimation Based on the Modal Model (ML-MM)

Before showing the results obtained by the new solver, a brief theoretical overview of the method is reported below. Then the results are shown and summarized.
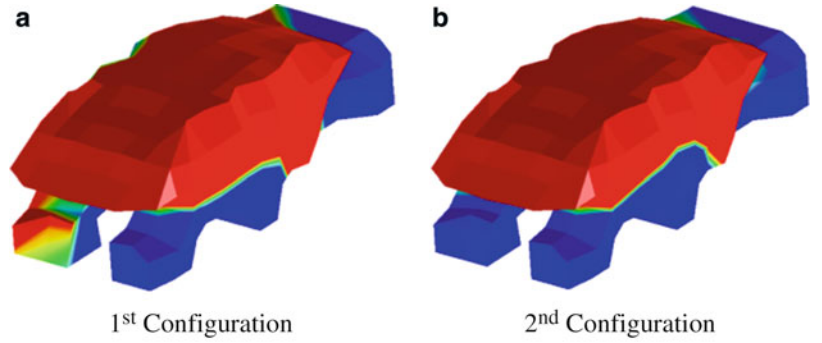
Fig. 4.25 I vertical mode

1st Configuration   2nd Configuration

Table 4.3 Comparison of modal parameters

6 references			10 references			12 references			
#	Frequency [Hz]	Damping [%]	#	Frequency [Hz]	Damping [%]	#	Frequency [Hz]	Damping [%]	Mode shape
2	53.36	14.46	2	53.72	15.38	2	52.54	12.89	I longitudinal
3	77.78	11.79	3	78.71	11.67	3	78.12	12.46	I longitudinal & rigid body trunk
4	95.61	8.43	4	95.91	8.72	4	96.08	9.22	I lateral
5	139.15	7.48	5	139.21	7.05	5	138.04	6.31	II longitudinal & rigid body trunk
			6	148.26	6.48	8	149.97	4.72	I longitudinal & I lateral
6	149.79	11.47	7	149.60	10.34	6	145.74	11.72	I vertical
7	151.41	6.46	8	149.82	9.27	7	148.37	9.24	I longitudinal & I lateral & I lateral trunk
8	192.86	6.34	9	194.21	6.74	9	194.22	7.82	III longitudinal
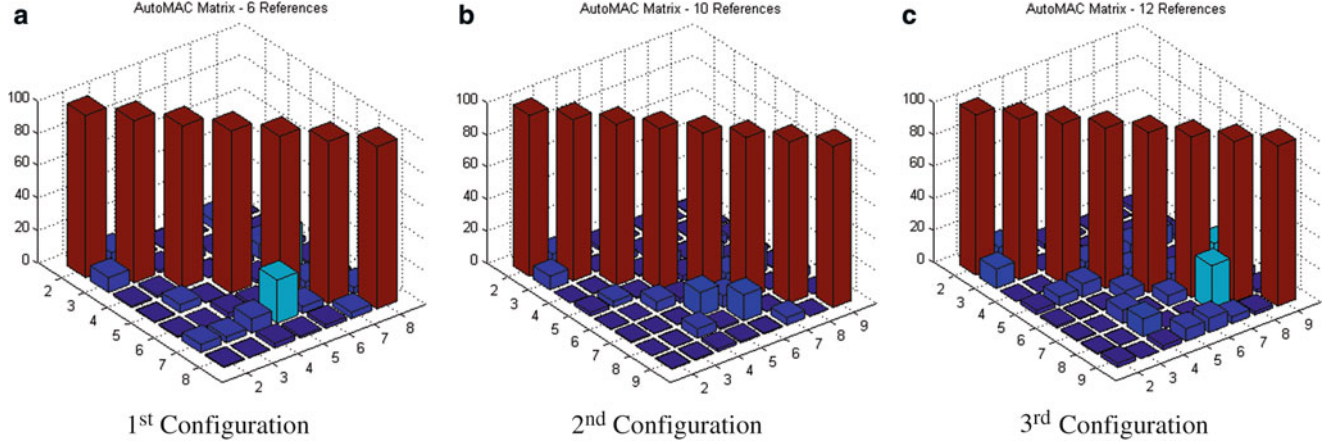
Fig. 4.26 AutoMAC for different configurations

4.4.2.1 Theoretical Background

The ML-MM method [7, 8, 21] is a multiple-input multiple-output (MIMO) frequency-domain estimator providing global estimates of the modal model parameters. In the first step of the ML-MM estimator, initial values of all the modal parameters (i.e. poles, mode shapes, participation factors, and upper and lower residuals) have to be specified. In the next step, the error between the modal model equation and the measured data is minimized in a maximum likelihood sense. Assuming the different measured FRFs to be uncorrelated, the ML-MM cost function to be minimized can be formulated as:

$$K_{ML-MM}(\theta) = \sum_{o=1}^{N_0} \sum_{k=1}^{N_f} E_o(\theta, \omega_k) E_o^H(\theta, \omega_k)$$

(4.7)
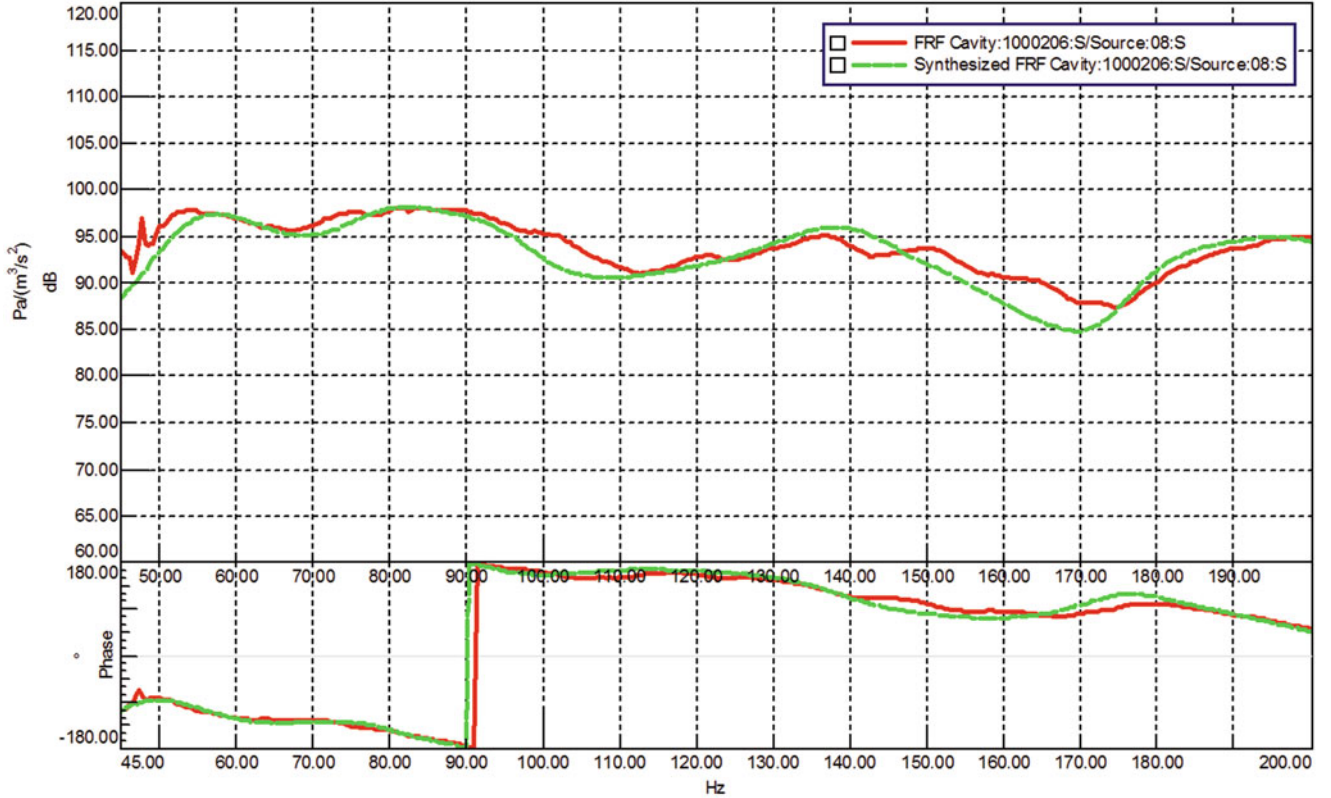
Fig. 4.27 Example of synthetized curve

where $()^H$ stands for the complex conjugate transpose of a matrix (Hermitian), N_o the number of outputs, N_f the number of frequency lines, ω_k the circular frequency, and $E_o(\theta, \omega_k)$ the weighted error equation corresponding to the o -th output degree of freedom (DOF) given as follows:

$$E_o(\theta, \omega_k) = \left[\frac{H_{o1}(\omega_k) - \widehat{H}_{o1}(\theta, \omega_k)}{\sqrt{var(H_{o1}(\omega_k))}} \cdots \frac{H_{oN_i}(\omega_k) - \widehat{H}_{oN_i}(\theta, \omega_k)}{\sqrt{var(H_{oN_i}(\omega_k))}} \right] \in C^{1 \times N_i} \tag{4.8}$$

where $H_{oi}(\omega_k) \in C$ the measured FRF, $\widehat{H}_{oi}(\theta, \omega_k) \in C$ the modeled FRF, $var(H_{oi}(\omega_k))$ the variance of the measured FRF for output o and input i and N_i is the number of inputs.

Assuming displacement FRFs, $\widehat{H}(\theta, \omega_k) \in C^{N_o \times N_i}$ can be represented using the modal model formulation as follows:

$$\widehat{H}(\theta, \omega_k) = \sum_{r=1}^{N_m} \left(\frac{\psi_r L_r}{s_k - \lambda_r} + \frac{\psi_r^* L_r^*}{s_k - \lambda_r^*} \right) + \frac{LR}{s_k^2} + UR \tag{4.9}$$

with N_m the number of identified modes, $\psi_r \in C^{N_o \times 1}$ the r -th mode shape, λ_r the r -th pole, $s_k = j\omega_k$, $()^*$ stands for the complex conjugate of a complex number, $L_r \in C^{1 \times N_i}$ the r -th participation factor, $LR \in C^{N_o \times N_i}$ and $UR \in C^{N_o \times N_i}$ the lower and upper residual terms. The lower and upper residual terms are modeling the influence of the out-of-band modes in the considered frequency band. The maximum likelihood estimates of θ (i.e. $\psi_r, L_r, \lambda_r, LR$, and UR) will be obtained by minimizing the above-mentioned cost function $k_{ML-MM}(\theta)$. This will be done using the Gauss-Newton optimization algorithm. To ensure convergence, the Gauss-Newton optimization is implemented together with the Levenberg-Marquardt approach, which forces the cost function to decrease [22]. To start the optimization algorithm, initial values for all the modal parameters are estimated by LMS Polymax method. More details about the ML-MM method (e.g. mathematical implementation, uncertainty derivation, ...) are presented in [7, 8, 21].

Table 4.4 Comparison of modal parameters

Polymax			ML-MM			
#	Frequency [Hz]	Damping [%]	#	Frequency [Hz]	Damping [%]	Mode shape
2	52.54	12.89	2	51.06	13.82	I longitudinal
3	78.12	12.46	3	81.44	14.94	I longitudinal & rigid body trunk
4	96.08	9.22	4	97.24	10.65	I lateral
5	138.04	6.31	5	137.79	7.25	II longitudinal & rigid body trunk
6	145.74	11.72	6	148.66	13.70	I vertical
7	148.37	9.24	8	150.74	11.79	I longitudinal & I lateral & I lateral trunk
8	149.97	4.72	7	149.34	6.57	I longitudinal & I lateral
9	194.22	7.82	9	195.13	6.05	III longitudinal

4.4.2.2 Results and Comparison

Modal parameters are again extracted using a total of 526×12 FRFs simultaneously. The analysis was stopped after 20 iterations.

As visible in Fig. 4.28, the curve fit improves drastically, with a mean fitting error around 2 %. Again nine pure acoustic modes are well identified in this frequency range. As visible in Table 4.4 and Fig. 4.29, the extracted modes are perfectly in line with those already estimated by Polymax, but the quality of the mode shapes seems to increase in terms of symmetry and similarity with the numerical ones. The AutoMAC matrix in Fig. 4.30b shows a really good independency of the eigenvectors estimated by ML-MM. It is also observed that the out of diagonal elements have lower values with respect to those from the AutoMAC matrix obtained with Polymax (Fig. 4.30a). Looking at Table 4.4 and Fig. 4.31, one can observe that the 7th and 8th modes are reversed in the two analyses. Some differences between Polymax and the ML-MM method can be seen in terms of the frequencies and damping estimates. Actually, these differences are reflected as an improvement in the goodness of the fit between the measured and the synthesized FRFs.

4.5 Conclusions

In this paper an intensive test campaign carried out to characterize the interior acoustic field of an automotive cabin is presented. Equipment and test procedure are described in detail. A CAE model of the cavity was used to study the optimal source distribution in order to place the exciters close to the antinodes. The geometry of the measurement points was also initially defined with the help of the CAE model and afterwards based on the true microphone locations. Such an FE model proved extremely useful both to quantify the influence of the Q-LMF sources on the interior acoustic field and to serve as a baseline on the expected pure acoustic modes. Once the measurement chain was validated, FRFs were measured between 526 microphones on roving arrays and 12 sources switched on sequentially.

Modal parameters are estimated in the frequency range between 40 and 200 Hz by two different methods: Polymax and ML-MM. Ten acoustically dominant modes are identified by both methods and seem to be in line with the numerical ones in terms of mode shapes. The modes extracted by the two methods are really comparable, although their order is reversed in some case. Nevertheless, ML-MM provides superior FRF synthesis results and, hence, more reliable values, as also shown by the more "natural" and symmetric mode shapes.

A study on the number of sources to be used in order to identify properly the acoustically dominant modes is reported as well. It has been observed that, whereas the lower modes (up to 140 Hz) are always well identified, the extraction of higher modes requires a large amount of sources. This is even more true when modes are present that are closely spaced in frequency.

Future studies will consist in further numerical analyses in order to better understand and quantify the vibro-acoustic coupling effects and the actual role of the damping in such a system. Updating of the acoustic cavity FE model based on test results, is also a very challenging task and subject of future investigations.
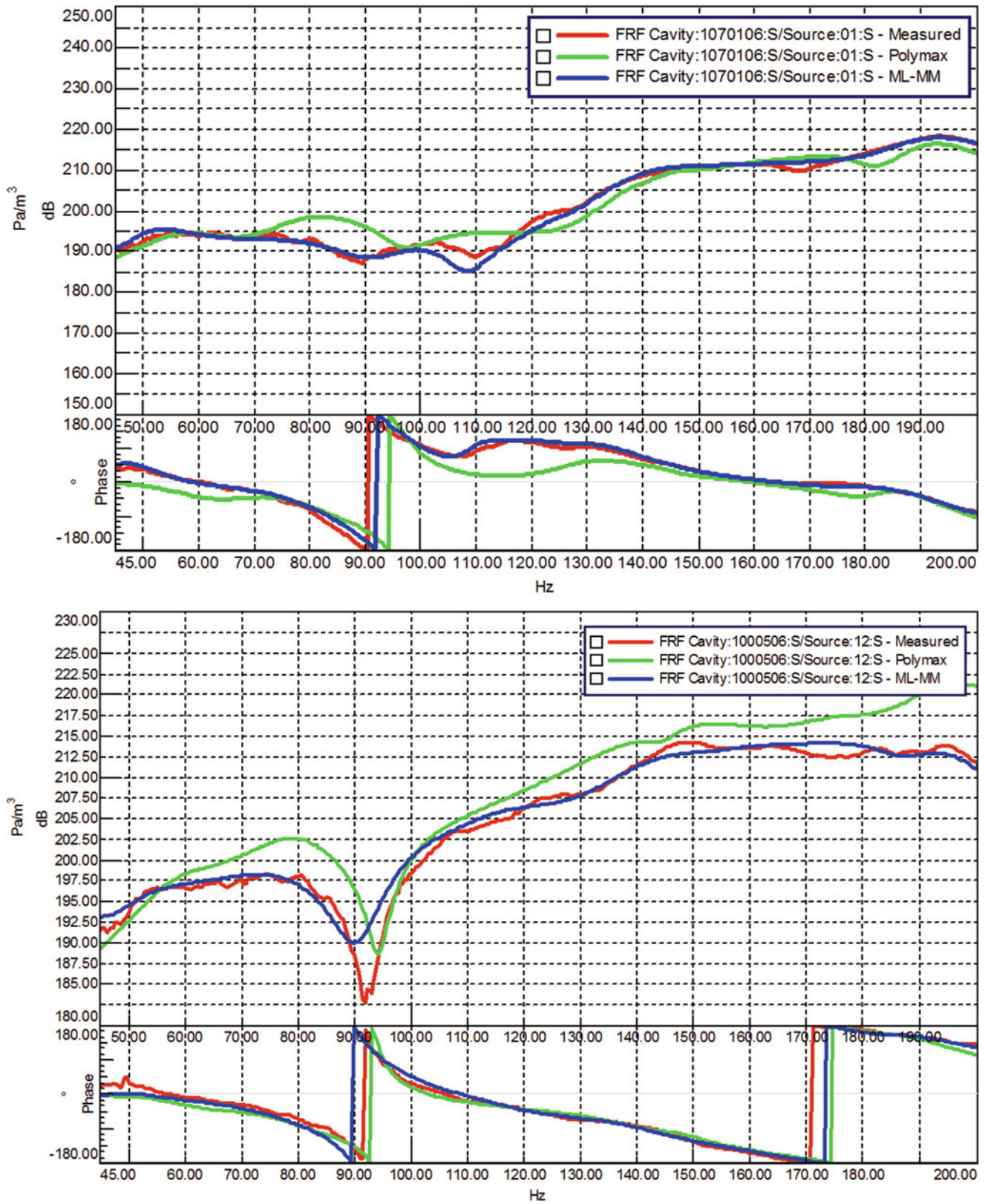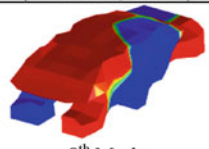
Fig. 4.28 Improved curve fitting
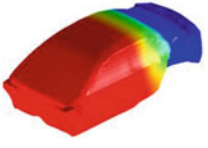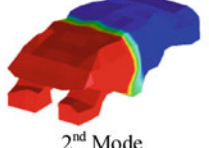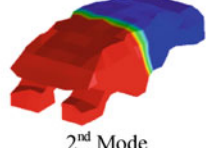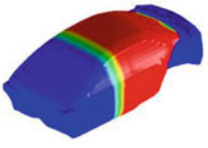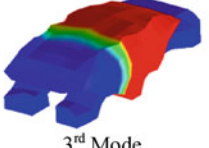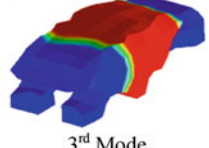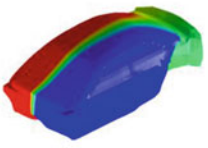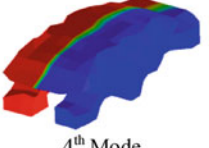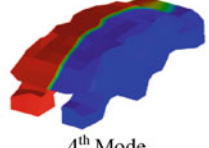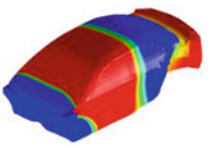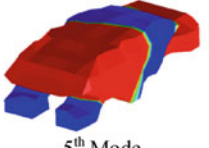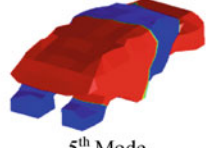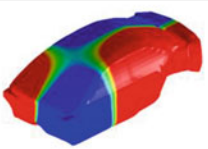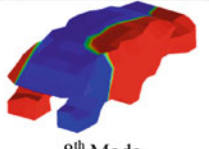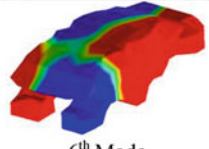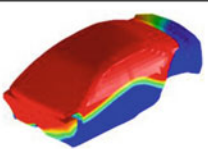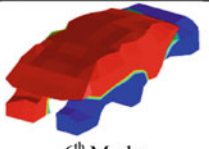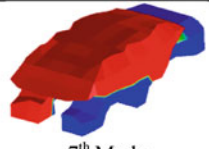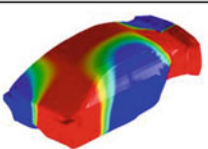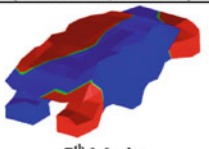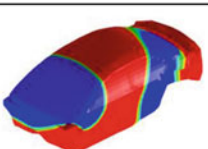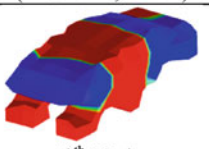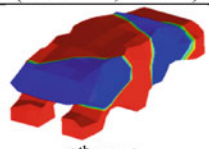
Numerical Modes (CAE Model)	Experimental Modes (Polymax)	Experimental Modes (ML-MM)	Mode Shape
	2nd Mode (52.54 Hz, 12.89%)	2nd Mode (51.06 Hz, 13.82%)	I Longitudinal
	3rd Mode (78.12 Hz, 12.46%)	3rd Mode (81.44 Hz, 14.94%)	I Longitudinal & Rigid Body Trunk
	4th Mode (96.08 Hz, 9.22%)	4th Mode (97.24 Hz, 10.65%)	I Lateral
	5th Mode (138.04 Hz, 6.31%)	5th Mode (137.79 Hz, 7.25%)	II Longitudinal & Rigid Body Trunk
	8th Mode (149.97 Hz, 4.72%)	6th Mode (148.66 Hz, 13.70%)	I Longitudinal & I Lateral & I Lateral Trunk
	6th Mode (145.74 Hz, 11.72%)	7th Mode (149.34 Hz, 6.57%)	I Vertical
	7th Mode (148.37 Hz, 9.24%)	8th Mode (150.74 Hz, 11.79%)	I Longitudinal & I Lateral & I Lateral Trunk
	9th Mode (192.22 Hz, 7.82%)	9th Mode (195.13 Hz, 6.05%)	III Longitudinal

Fig. 4.29 Mode shapes – comparison (The discrepancies between the CAE and test geometry in the front part of the cavity are not due to a different modelling of the car. The region between the foot area and the dashboard is present in the real scenario as well, but hardly accessible to the sensors)
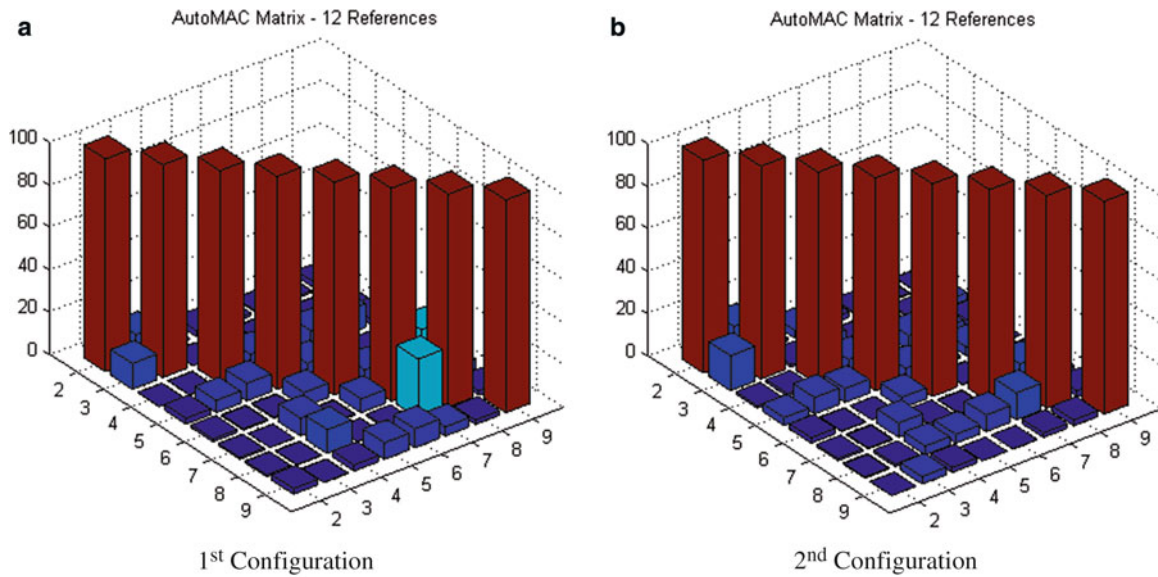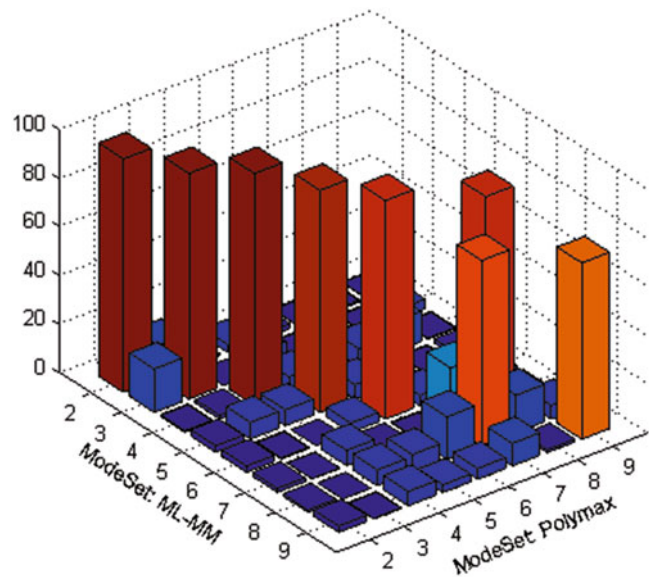
Fig. 4.30 AutoMAC matrices

Fig. 4.31 MAC between Polymax and ML-MM

References

1. Sung TMSH, Nefske DJ, Le-The H, Bonarens F (1999) Development and experimental evaluation of a vehicle structural-acoustic trimmed-body model. SAE technical paper 1999-01-1798
2. Sanderson MA, Onsay T (2007) CAE interior cavity model validation using acoustic modal analysis. SAE technical paper 2007-01-2167
3. Peeters B, El-kafafy M, Accardo G, Knechten T, Janssens K, Lau J, Gielen L (2014) Automotive cabin characterization by acoustic modal analysis. In: Proceedings of JSAE spring annual conference, Yokohama, Japan 114–20145437
4. Yoshimura T, Saito M, Maruyama S, Iba S (2012) Modal analysis of automotive cabin by multiple acoustic excitation. In: Proceedings of ISMA, Leuven, Belgium
5. Tsuji H, Maruyama S, Yoshimura T, Takahashi E (2013) Experimental method extracting dominant acoustic mode shapes for automotive interior acoustic field coupled with the body structure. SAE technical paper 2013-01-1905
6. Peeters B, Van der Auweraer H, Guillame P, Leuridan J (2004) The PolyMAX frequency-domain method: a new standard for madal parameter estimation. Shock Vib 11:395–409
7. El-Kafafy M, De Troyer T, Peeters B, Guillame P (2013) Fast maximum-likelihood identification of modal parameters with uncertainty intervals: a modal model-based formulation. Mech Syst Sign Proc 37:422–439
8. El-Kafafy M, Guillame P, De Troyer T, Peeters B (2012) A frequency-domain maximum likelihood implementation using the modal model formulation. In: Proceedings of SYSID, Brussels

9. Fahy F, Gardonio P (1985) Sound structural vibration. Radiation, transmission and response. Academic, London
10. Ohayon R, Soize C (1998) Structural acoustics and vibration. Mechanical models, variational formulations and discretizations. Academic, London
11. Dhandole S, Modak SV (2012) A constrained optimization based method for acoustic finite element model updating of cavities using pressure response. Appl Math Model 36:399–413
12. Heylen W, Lammens S, Sas P (2012) Modal analysis. Theory and testing. PMA – K.U. Leuven, Belgium
13. Wyckaert K, Augusztinovicz F, Sas P (1996) Vibro-acoustical modal analysis: reciprocity, model symmetry, and model validity. J Acoust Soc Am 100(5):3172–3181
14. Xu H, Dickinsons O, Wang J, Kang H (2014) Acoustic cavity modal analysis for NVH development of road machinery cabins. In: Proceedings of the 32nd international modal analysis conference, Orlando
15. Tsuji H, Enomoto T, Maruyama S, Yoshimura T (2012) A study of experimental acoustic modal analysis of automotive interior acoustic field coupled with the body structure. SAE technical paper 2012-01-1187
16. Brandt A (2011) Noise and vibration analysis: signal analysis and experimental procedures. Wiley, Hoboken, West Sussex, UK
17. Wyckaert K, Meulewaeter L (1996) On the influence of finite acoustic source dimensions on acoustical frequency response funcions inside an enclosed cavity. In: Proceedings of ISMA, Leuven, Belgium
18. Coster C, Nagahata D, van der Linden PJG (2010) On the accuracy reciprocal and direct vibro-acoustic transfer-function measurements on vehicles for lower and medium frequencies. In: Proceedings of ISMA, Leuven, Belgium
19. He J, Fu ZF (2001) Modal analysis. Butterworth-Heinemann, Oxford
20. Ewins DJ (2000) Modal testing: theory, practice and application. Research Studies Press Ltd, Philadelphia
21. El-kafafy M, Accardo G, Peeters B, Janssens K, De Troyer T, Guillame P (2015) A fast maximum likelihood-based estimation of a modal model. In: Proceedings of the 33rd international modal analysis conference, Orlando
22. Eykhoff P (1979) System identification: parameter and state estimation. Wiley, Bristol